

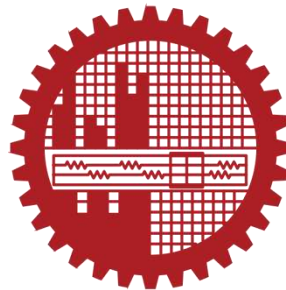
SELF-CLEANING PROPERTY ENHANCEMENT OF NANO-TiO₂ PARTICLES BY DOPING WITH IRON

by

Md. Johirul Islam

Student ID: 1015172007

**MASTER OF SCIENCE IN
GLASS AND CERAMIC ENGINEERING**



Department of Nanomaterials and Ceramic Engineering


BANGLADESH UNIVERSITY OF ENGINEERING AND TECHNOLOGY

Dhaka-1000, Bangladesh


February, 2023

The thesis titled “**SELF-CLEANING PROPERTY ENHANCEMENT OF NANO-TiO₂ PARTICLES BY DOPING WITH IRON**” submitted by Md. Jahirul Islam, Roll No.: 1015172007, Session: October 2015, has been accepted as satisfactory in partial fulfillment of the requirement for the degree of Master of Science in Glass and Ceramic Engineering on 27 February 2023.

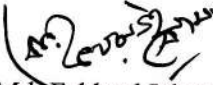
BOARD OF EXAMINERS

- 


1. Dr. Muhammad Hasanuzzaman
Associate Professor
Department of Nanomaterials and Ceramic Engineering
BUET, Dhaka-1000

Chairman
(Supervisor)
- 


2. Dr. Md. Abdullah Zubair
Associate Professor and Head
Department of Nanomaterials and Ceramic Engineering
BUET, Dhaka-1000

Member
(Ex- officio)
- 

3. Dr. Md. Pakhrul Islam
Professor
Department of Nanomaterials and Ceramic Engineering
BUET, Dhaka-1000

Member
- 

4. Dr. Md. Abdullah Zubair
Associate Professor
Department of Nanomaterials and Ceramic Engineering
BUET, Dhaka-1000

Member
- 

5. Dr. Fahmida Gulshan
Professor
Department of Materials and Metallurgical Engineering
BUET, Dhaka-1000

Member
(External)

CANDIDATE'S DECLARATION

It is hereby declared that except where specified by reference to other works, the studies embodied in this thesis are the results of investigation carried out by the author under the supervision of Dr. Muhammad Hasanuzzaman, Associate Professor, Department of Nanomaterials and Ceramic Engineering, BUET. Neither the thesis nor any part of it has been submitted elsewhere for any other purposes.



Md. Jahirul Islam

Roll No.: 1015172007

DEDICATION

I dedicate this thesis to my beloved parents and family members.

ACKNOWLEDGMENT

This endeavor would not have been possible without the help of numerous individuals, to whom I am extremely appreciative. First and foremost, I would like to express my deepest gratitude to my supervisor **Dr. Muhammad Hasanuzzaman** for his invaluable supervision, continuous support, patience, and tutelage throughout this degree.

I am also grateful to **Dr. Md. Fakhru Islam** for allowing me to work in the Nanomaterials and Ceramic Engineering Department. I would like to extend my sincere thanks to **Dr. Md. Abdullah Zubair, Dr. Md. Saiful Islam, and Ms. Manifa Noor** for their support and inspiration during my M.Sc. study.

Special thanks to **Mr. Md. Farabi Rahman, Ms. Mobashera Saima Haque, and Mr. Md. Shahjalal Rana** for their help during the characterization of my samples.

I am also thankful to all the faculty members, and technical and official staff of the **Department of Nanomaterials and Ceramic Engineering, BUET** for their assistance and cooperation during this whole time. I would also like to gratefully acknowledge the Committee for Advanced Studies & Research (CASR), Bangladesh University of Engineering and Technology (BUET) for financing this research.

Finally, I want to thank my friend **Mr. Mohammad Arif Mokammel** for his help in proofreading and my family members for their mental support.

Table of Contents

Acknowledgment	v
List of Tables	viii
List of Figures	ix
List of Abbreviations, Technical Symbols and Terms.....	xi
Abstract	xiii
CHAPTER 1: INTRODUCTION	1
1.1 Background and Motivation of the Research.....	1
1.2 Mechanism of Self-cleaning	2
1.3 Current Challenges for Self-cleaning.....	5
1.4 Objective of this Research	7
1.5 Thesis Overview	8
CHAPTER 2: LITERATURE REVIEW	9
2.1 Nanomaterials Introduction	9
2.2 Properties of Nanomaterials.....	9
2.2.1 Quantum Tunneling	10
2.2.2 Quantum Confinement.....	10
2.2.3 Optical Properties.....	12
2.2.4 Surface Properties and Shape also Matters	13
2.3 Uses of Nanomaterials	13
2.4 Electronic and Crystal Structures of TiO ₂	14
2.5 Modification Technique of TiO ₂	16
2.6 Photocatalytic Activity of Fe-doped TiO ₂	19

2.7 Notable Scholarly Works Regarding Fe-doped TiO ₂	20
2.8 Applications of TiO ₂ Nanoparticles	26
CHAPTER 3: EXPERIMENTAL METHODOLOGY.....	39
3.1 Materials Synthesis	39
3.2 Characterization of the Undoped and Fe-doped TiO ₂ Samples	42
3.2.1 FESEM Analysis.....	43
3.2.2 X-Ray Diffraction Analysis	43
3.2.3 UV-Visible Spectroscopy Analysis	43
3.2.4 Photocatalytic Dye Degradation Experiment.....	43
3.2.5 Hydrophilic Conversion Test	45
CHAPTER 4: RESULTS AND DISCUSSION.....	46
4.1 Morphology Analysis by FE-SEM	46
4.2 Structural Analysis by X-Ray Diffraction	49
4.3 Optical Analysis by UV-Vis Spectroscopy.....	53
4.4 Photocatalytic Activity Analysis by Methylene Blue Degradation	57
4.5 Hydrophilicity Comparison.....	59
CHAPTER 5: CONCLUSIONS AND FUTURE WORK.....	63
5.1 Conclusions.....	63
5.2 Future Work	64
REFERENCES	65

LIST OF TABLES

Table 1.1: Comparison properties of hydrophilicity and hydrophobicity	6
Table 4.1: Average particle sizes of pure and Fe-doped TiO ₂ samples	46
Table 4.2: The Bragg angles and the corresponding crystallographic planes of obtained sample confirm the anatase phase	51
Table 4.3: Comparison of average crystallite size obtained from XRD and average particle size from SEM	52
Table 4.4: Photocatalytic Degradation of MB solution	59
Table 4.5: Contact angles of the water droplets on the undoped, Fe-doped TiO ₂ coated, and uncoated glass surfaces under UV and visible light illumination	60
Table 4.6: Overall comparison of undoped, Fe _{0.01} , Fe _{0.02} , Fe _{0.03} , and Fe _{0.04} doped TiO ₂	62

LIST OF FIGURES

Figure 1.1: The photocatalytic activity of TiO ₂ under UV irradiation.	4
Figure 1.2: Schematic illustration for the band gap structure showing the CB and VB positions of TiO ₂ and the redox potentials vs. NHE.....	5
Figure 2.1: Schematic representation of tunneling.	10
Figure 2.2: Band diagram of Insulator, semiconductor, and conductor.	11
Figure 2.3: Illustration of quantum confinement effect..	12
Figure 2.4: (a) Crystal Structure of anatase where Ti atoms are grey and O atoms red. (b) Equilibrium crystal shape of anatase TiO ₂ through Wulff construction	15
Figure 2.5: Molecular-orbital bonding structure for anatase TiO ₂ :(a) Atomic levels (b) Crystal-field split levels (c) Final interaction states.	16
Figure 2.6: Three schemes for band gap modifications for visible-light sensitization: (a) Lower shift of CBM (b) A higher shift of VBM (c) Introduction of impurity states.	17
Figure 2.7: Mechanism of TiO ₂ photocatalysis. hv ₁ : pure TiO ₂ ,hv ₂ : metal-doped TiO ₂ , hv ₃ : nonmetal-doped TiO ₂	18
Figure 2.8: Schematic representation of mechanism involved in photocatalytic activity of Fe-doped TiO ₂	20
Figure 2.9: Photocatalytic degradation of MB for samples of (a) N-Fe-TiO ₂ , (b) Fe-TiO ₂ , (c) N-TiO ₂ , (d) P-25, (e) TiO ₂ . reference.	22
Figure 2.10: Photocatalytic degradation of RB 4 dye with synthesized catalysts; C ₀ =10 ppm, catalyst amount= 0.24gm/200ml. reference.....	26
Figure 2.11: Glass covers on highway tunnel lighting fixtures darkened by automobile exhaust without TiO ₂ and maintained clean with TiO ₂	30
Figure 2.12: Anti-fogging effect of automobile side-view mirror: conventional mirror (left) and TiO ₂ -coated hydrophilic mirror (right).	38
Figure 3.1: Schematic process for the synthesis of undoped and Fe-doped TiO ₂	40

Figure 3.2: Physical appearances of undoped and Fe-doped TiO ₂ at different steps of synthesis: (i) After gel formation; (ii) After drying; (iii) After grinding and annealing..	41
Figure 3.3: Photocatalyst-coated glass surfaces.	42
Figure 3.4: Prepared box with the arrangement of UV-A and visible light bulbs for checking the photocatalytic activity of the samples.	44
Figure 4.1: FE-SEM images of the samples at magnification x 100,000. (A) Undoped TiO ₂ (B) Fe _{0.01} doped TiO ₂ (C) Fe _{0.02} doped TiO ₂ (D) Fe _{0.03} doped TiO ₂ (E) Fe _{0.04} doped TiO ₂	49
Figure 4.2: XRD patterns of undoped and Fe-doped TiO ₂ samples. All Bragg peaks are indexed according to their corresponding crystallographic planes.	50
Figure 4.3: UV-Vis absorbance spectra of the samples. (A) Undoped TiO ₂ (B) Fe _{0.01} doped TiO ₂ (C) Fe _{0.02} doped TiO ₂ (D) Fe _{0.03} doped TiO ₂ (E) Fe _{0.04} doped TiO ₂	56
Figure 4.4: Photocatalytic activities of undoped and Fe-doped TiO ₂ samples: (A) photocatalytic degradation of MB solution indicated as C/C ₀ (C ₀ = 20 ppm MB solution), (B) MB degradation percentage as a function of irradiation time.	58

LIST OF ABBREVIATIONS, TECHNICAL SYMBOLS AND TERMS

ADH-1	A cyclic pentapeptide vascular-targeting drug
C@TiO ₂	TiO ₂ nanoparticles wrapped by graphitic carbon
CB	Conduction band
CBM	Conduction band minimum
CD44	A non-kinase transmembrane glycoprotein
CE	Coulomb efficiency
DNA	Deoxyribonucleic acid
DOX	Doxorubicin
E _g	Band gap
EG	Ethylene glycol
eV	Electronvolt
FDA	Food and Drug Administration
FE-SEM	Field emission scanning electron microscopy
FT-IR	Fourier transform infrared
g-C ₃ N ₄	Graphitic carbon nitrides
HD	High definition
ICD	Indigo carmine dye
LED	Light emitting diode
MB	Methylene blue
MO	Methyl orange
MTN	Mesoporous titania nanoparticles
NCQD	N-doped carbon quantum dots
NHE	Normal hydrogen electrode
NPs	Nanoparticles
P-25	Degussa

P-25	Titanium dioxide nanopowder
PAM	Polyacrylamide
PEG	Polyethylene glycol
PES	Polyester
QD	Quantum dot
RB 4	Reactive Blue 4 dye
ROS	Reactive oxygen species
TBT	Tetrabutyl titanate
Ti@TiO ₂	TiO ₂ nanowire array and the Ti wire substrate
TTIP	Titanium tetraisopropoxide
UV	Ultraviolet
UV-vis	Ultraviolet and visible
VB	Valence band
VBM	Valence band maximum
V _o	Oxygen vacancy
VOCs	Volatile organic compounds
XAFS	X-ray absorption fine structure
XRD	X-ray diffraction

ABSTRACT

Among all nanoparticle types, TiO₂ (anatase) has proven to be the most promising one, primarily because of its superhydrophilic properties and effective antibacterial actions. The photo-induced self-cleaning characteristic can be demonstrated by the hydrophilicity of TiO₂ nanoparticles. However, the lack of photosensitivity to visible light (>390 nm) reduces the scope for utilizing TiO₂ in photocatalytic processes. Therefore, most studies regarding TiO₂ nanoparticles have focused to broaden its spectral sensitivity through band gap manipulation for effective photocatalysis under visible light. Transition metal dopants have been used to decrease the band gap energy of TiO₂ for visible light-responsive photocatalytic purposes. Fe³⁺ is a good dopant candidate for producing visible light-sensitive nanoparticles owing to its capability to decrease the band gap energy and enhance electron/hole trapping. In this study, nanocrystalline undoped and Fe-doped TiO₂ (Ti_{1-x}Fe_xO₂, x = 0.01 to 0.04) was synthesized by the sol-gel method. The prepared samples were characterized by X-ray diffraction (XRD), field emission scanning electron microscopy (FE-SEM), and ultraviolet and visible spectroscopy (UV-vis) to study their structure, morphology, and optical properties. A photocatalytic dye degradation test and a hydrophilic conversion test were carried out to compare the photocatalytic activity and hydrophilicity of the samples under UV and visible light. The obtained results demonstrated the self-cleaning characteristic of undoped and Fe-doped TiO₂ nanoparticles. According to the characterizations and comparisons of the prepared samples, particle size and band gap reduction were observed due to an increase in Fe concentration in Fe-doped TiO₂, which yielded a red shift in the absorption band edge. Fe_{0.03}-doped TiO₂ (average particle size 21.3 nm, crystallite size 11.97 nm, and band gap 2.37 eV) showed the optimum photocatalytic activity (60% MB degradation) and super-hydrophilicity (water droplet contact angle 9°) under visible light radiation. This optimum result was possible because the band gap reduction of Fe-doped TiO₂ reached an optimum level in Fe_{0.03}-doped TiO₂ so that more (\cdot OH) radicals and (O_2^-) groups were produced by achieving the optimum number of electron- and hole-trapping sites and the lowest rate of electron-hole recombination. Further increase of Fe content (Fe_{0.04}-doped TiO₂) increased the electron-hole recombination center, hence an increment of the rate of recombination which yielded lower photocatalytic reaction and hydrophilicity. Therefore, Fe_{0.03}-doped TiO₂ was found to be the optimum doping content that can effectively be used as self-cleaning coating material.

CHAPTER 1: INTRODUCTION

1.1 Background and Motivation of the Research

Titanium dioxide (TiO_2) is a non-toxic naturally occurring transition metal oxide of titanium. The TiO_2 nanoparticles have significant properties because the quantum effect dominates the regular physics of material [1]. Generally, TiO_2 is used as a whitening agent in paints, toothpaste, cosmetics, and many more. Nano- TiO_2 particles have a higher surface-to-volume ratio and more exposed surface area than that bulk- TiO_2 . In TiO_2 nanocrystals, the confinement of the charges tends to have discrete energy states which are responsible for unique properties [2]–[4]. These properties provide unique solutions to various technological problems. Nano- TiO_2 has been widely used for the last two decades as a water and air purifier [5], antibacterial agent [6], self-cleaning and hydrophilic glass and ceramic surfaces [7]. A number of researches have been carried out to utilize the photocatalytic characteristic of TiO_2 after the discovery of photocatalytic water splitting on TiO_2 electrodes under ultraviolet (UV) light by Fujishima and Honda [8]. Solid surfaces coated with TiO_2 nanoparticles show high hydrophilicity when exposed to lights of specific wavelengths. Electrons and holes produced by the photocatalytic reactions of TiO_2 play a vital role in decomposing organic compounds. There are three polymorphs of TiO_2 which are anatase, rutile and brookite. Generally, anatase displays much higher photocatalytic activities than both rutile and brookite [9]. As the photocatalytic activities of anatase is activated under ultraviolet light ($\lambda < 390$ nm), which is present only about 3% in sunlight, the photocatalytic characteristic of TiO_2 is inactive under visible light [10].

To develop visible-light sensitization and a more efficient photocatalyst, band gap modification of TiO_2 has been done by doping and co-doping of non-metals or metals in TiO_2 [11]–[14]. Doping and co-doping can be defined as the addition of a small amount of impurity or extraneous materials to nanoparticles to impart suitable properties to them. Among the various combinations of non-metal and metal doping, iron has received considerable attention because of its interesting effect in depressing the

electron-hole recombination rate, which is the prime condition for increasing photocatalytic activities [15]. Moreover, with this modification, the hydrophilicity of the TiO₂-coated surfaces can also be increased. Hydrophilicity is one of the prime factors to increase the wettability of the TiO₂-coated self-cleaning surfaces. However, an adequate comparative study is so far lacking on the hydrophilic properties of this dopant TiO₂-coated surface. This research work was focused on the comparative influence of undoped and Fe-doped TiO₂-coated glass surfaces in the visible region. Since LED light is used as the common source of indoor light nowadays, it was used as a visible light source during the study under the visible region. The study of the photo catalytic activity of Fe-doped TiO₂ under LED light is a unique aspect of this work.

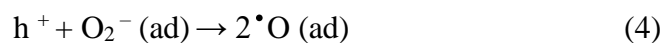
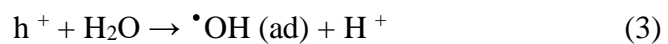
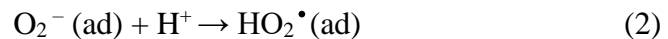
1.2 Mechanism of Self-cleaning

Self-cleaning can be achieved by both hydrophilicity and hydrophobicity of surfaces. The wettability of a surface plays an important role in self-cleaning. It can be determined by the contact angle between the surface and the water droplet at the solid-vapor-liquid interface. The contact angle of a liquid droplet deposited on a solid depends not only on the surface morphology but also on external parameters such as temperature, humidity, light, etc. A change in these parameters may propel the transition from partial wetting to complete wetting of the surface. Self-cleaning induced by hydrophilicity was explored in this research work.

The hydrophilic nature of solid surfaces is a widely researched topic in materials science because of its usefulness and future commercial potential. Under the light of definite wavelengths, these surfaces take part in photocatalysis and cause the dirt materials to decompose [16]. The water molecules then wash away the dirt particles along their path and clean the surface. These surfaces are synthesized by applying a coating that is composed mostly of metal oxide. Studies have revealed that metal oxides such as TiO₂, ZnO, SnO₂, and Al₂O₃ are useful for utilizing as coating material [17]–[19]. However, TiO₂ has received the focus among researchers because of its substantial photocatalytic activity, non-toxicity, cost-effectiveness, chemical stability, and

transparency. Furthermore, TiO₂ is used in textiles and painting as a pigment, in cosmetics as a blocker of UV rays, and is also known to have strong bactericidal properties [20]. Although the mechanism of hydrophilicity described in this thesis paper mainly focused on TiO₂, the process is similar for all other metal oxides used in self-cleaning applications.

The combined properties of photocatalysis and superhydrophilicity are the basis of the self-cleaning action of metal oxides. Photocatalytic activity degrades organic and inorganic contaminants in the presence of ultraviolet (UV) light. TiO₂ mainly absorbs UV photons resulting in the generation of electrons and holes on the surface of the coated solid. A photon having energy equal to or higher than that of the band gap pushes an electron from the valence band to the conduction band and leaves behind a hole in the valence band [21]. The photogenerated electrons and holes either recombine or migrate to the surface. These migrated electrons and holes react with the contaminants present on the surface. The holes in the valence band also react with water molecules adsorbed on the surface to produce hydroxyl radicals ($\cdot\text{OH}$). On the other hand, the electrons in the conduction band reduce O₂ to produce superoxide ions (O₂⁻). Because of their strong oxidation power, hydroxyl radicals and superoxide ions are very active in decomposing organic compounds. The hydroxyl radicals ($\cdot\text{OH}$) on the surface of the TiO₂ increase the hydrophilic ('water-loving') character of the TiO₂-coated surfaces. Organic compounds are decomposed in the presence of water molecules on the surface of TiO₂. When it rains, the water runs off the TiO₂-coated surfaces in the form of a sheet, and the dirt is washed off. Therefore, relative humidity and oxygen content in the environment are two very important factors for hydrophilicity [22]. Products of the following reactions are responsible for the decompositions [23]:



Here, the first two reactions involve conduction band minimum (CBM) and the last two valence band maximum (VBM). Therefore, the band alignments of CBM and VBM with respect to the redox potentials for water are important criteria required to achieve the high photocatalytic activity.

Metal oxide surfaces are also advantageous because they show reversible wettability, meaning that they exhibit hydrophobicity upon storing in the dark and hydrophilicity when re-exposed to UV radiation [24]. The schematic representation of photocatalytic hydrophilicity in the case of TiO₂ films under UV irradiation is shown in **Figure 1.1**.

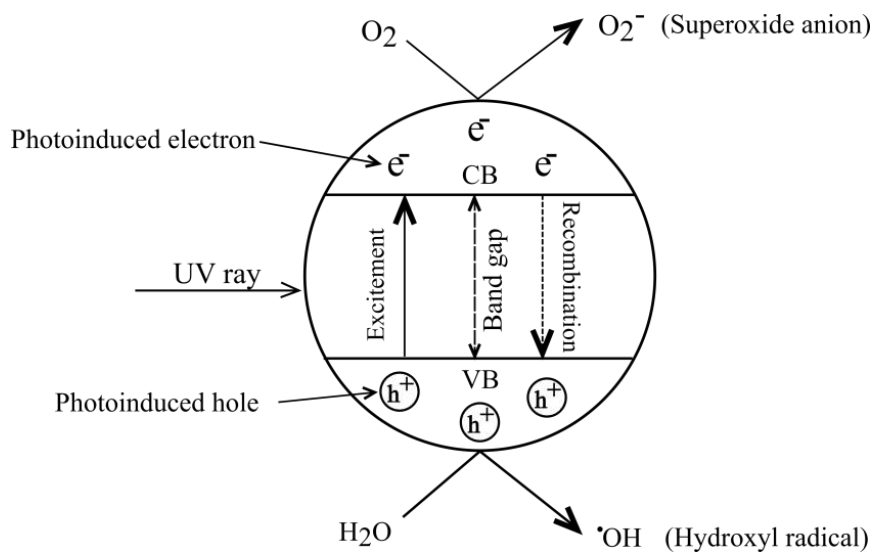


Figure 1.1: The photocatalytic activity of TiO₂ under UV irradiation. Modified from reference [21].

When the energy of the incident photons matches the band gap energy (E_g) of semiconductors, semiconductor oxide photocatalysts can absorb solar light. Thus, the electrons are excited from the valence band (VB) to its conduction band (CB) and initiate reduction reactions on the catalyst surface under solar radiation. Oxidation is caused by the holes left in the valence band. The electron-hole pairs recombine very fast and release energy in the form of heat when they are not used in photocatalytic

reactions. The electron-hole pairs are separated and diffused to the surface of the electrode. Redox reactions take place on photocatalyst surfaces [25]. There are many semiconductors oxide photocatalysts, among them, TiO_2 is an n-type semiconductor that shows optical absorption in the UV region ($\lambda < 390 \text{ nm}$) of the solar spectrum. Its CB level (-0.3 eV) is more negative and suitable for the redox potential of H^+/H_2 (0 eV) and its VB level (2.9 eV) is more positive than the standard redox potential of $\text{O}_2/\text{H}_2\text{O}$ (1.23 eV) as compared to a normal hydrogen electrode (NHE) as shown in **Figure 1.2**. electron-hole pairs are produced when TiO_2 is irradiated under solar light. The electrons in the CB reduce H^+ ions to evolve H_2 , and the holes in the VB oxidize H_2O to form O_2 [26].

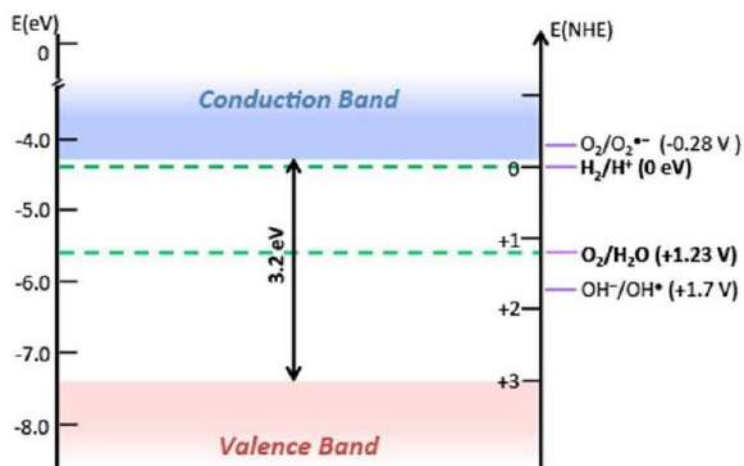


Figure 1.2: Schematic illustration for the band gap structure showing the CB and VB positions of TiO_2 and the redox potentials vs. NHE [26].

1.3 Current Challenges for Self-cleaning

Nanoscale materials are a relatively new topic of research but have high potential in various sectors such as electronics, cosmetics, textiles, medicine, ceramics, etc. The use of nanomaterials as a self-cleaning agent for solid surfaces is being researched widely and scientists have been able to suggest some outlines for developing a viable technology. The self-cleaning character of a surface can be induced by both

hydrophobicity and hydrophilicity [27], [28]. The property of hydrophobicity is seen in nature e.g., on lotus and rice leaves, legs of water striders, taro leaves, etc. The surface morphology of these leaves enables them to repel water and water droplets and simply sweep away the dirt particles along their path on these surfaces [29]. It is possible to simulate this mechanism just by making a surface with similar morphology [30]. On the other hand, self-cleaning characteristic by hydrophilicity is not a natural phenomenon. Proper designing and application of nanoscale materials are required to impart this character to solid surfaces. In general, solid surfaces do not have self-cleaning properties through hydrophilicity. A material (metal oxide like TiO₂ or ZnO) has to be added as a coating which activates self-cleaning properties in the presence of water molecules and light of specific wavelengths. However, this technique seems to work only under UV light which drastically limits its applications [21]. Comparisons of Self-cleaning properties induced by hydrophobicity and hydrophilicity are listed in **Table 1.1**.

Table 1.1: Comparison properties of hydrophilicity and hydrophobicity

Hydrophilicity	Hydrophobicity
(1) Hydrophilicity depends on the chemical composition of the surface coating.	(1) Hydrophobicity depends on the morphology or physical structure of the surface.
(2) Employs photocatalysis under the influence of light.	(2) Does not employ photocatalysis.
(3) Decomposes dirt materials.	(3) Does not decompose dirt materials.
(4) Not found in nature.	(4) Found in nature.
(5) Shows antimicrobial properties.	(5) Does not show antimicrobial properties.
(6) Requires light of specific wavelengths.	(6) Does not require light at all.
(7) Employs chemical reactions.	(7) Does not employ any chemical reaction.

The main challenge that scientists are dealing with nowadays is the activation of the self-cleaning ability of nanomaterials in the visible region of light. Proposals have been made to dope nano-sized metal oxides with either metal or non-metal to trigger their self-cleaning characteristics under visible light. Commercialization of this technology is only possible after overcoming this challenge.

Therefore, doping and co-doping of metal or non-metal in TiO₂ is required to activate the self-cleaning process under visible light. Researchers have used different materials to impart the hydrophilic self-cleaning property of TiO₂ to solid surfaces under visible light. It is a topic of great significance because of its useful applications in our homes, office buildings, and other belongings. With the successful application of this technology, glass windows of homes and cars, tiles, roofs, solar cells, and fabrics will be cleaned automatically under sunlight and visible light. It will make risky human labor unnecessary and also decrease the maintenance cost.

1.4 Objective of this Research

Nanotechnology has brought the era of the nano revolution. Every aspect of our life will be influenced by this nano revolution. Nano TiO₂ particles are used for building an energy-efficient, pollutant-free, and eco-friendly world. But, the uses of nano TiO₂ particles are limited under the light of UV region as it is not active under visible light. Therefore, the main objective of this research is to eradicate the limitation of nano TiO₂ by making it responsive to visible light.

This research aims to synthesize undoped and Fe-doped nano-TiO₂ (especially anatase) by sol-gel synthesis process and to produce a self-cleaning coating on glass surfaces by a dip coating method. Besides, a comparison of hydrophilicity among these photocatalyst-coated glass surfaces under UV radiation and visible light is also the aim of this research.

Objectives:

- To enable visible-light sensitization of nano-TiO₂ particles by doping.
- To increase the photocatalytic activity of nano-TiO₂ particles under visible light.
- To produce a self-cleaning coating of undoped and Fe-doped TiO₂ on glass surfaces.
- To compare the hydrophilicity between undoped and Fe-doped TiO₂-coated surfaces.

1.5 Thesis Overview

This thesis is divided into five chapters. Chapter 1 begins by laying out the background of this research, explaining the mechanism of self-cleaning, highlighting current challenges for self-cleaning, and pointing out the objectives and overview of the thesis paper. Chapter 2 starts with a brief review of nanomaterials, their basic properties, and their uses. Further in this chapter, a brief review of the crystal structure of TiO₂, its modification technique, notable scholarly works regarding Fe-doped TiO₂, and applications of TiO₂ nanoparticles are highlighted. Chapter 3 describes the experimental methodology which includes the synthesis of materials, preparation of photocatalyst-coated glass surfaces, characterization of the prepared samples, photocatalytic dye degradation experiment, and hydrophilic conversion test of photocatalyst-coated glass surfaces. The results of the characterization, experiments, and tests are presented and discussed in chapter 4. Finally, the conclusion of the thesis work is summarized, and the future scope of this research is disclosed in chapter 5.

CHAPTER 2: LITERATURE REVIEW

2.1 Nanomaterials Introduction

A nanoparticle is a small object that behaves like a whole unit that, in three-dimensional space, falls within the nanometer scale range (1–100 nm) or at least one of the dimensions is within this range [31]. In the case of pronouncing nanomaterials, at least half of the particles in the number size distribution must measure 100 nm or below according to the European Commission [32]. In other words, materials with grain sizes in the order of a billionth of a meter are called nanomaterials. Nanomaterials are a widely researched topic in the field of materials science because of their extraordinary properties. They can be modified and utilized to solve various technical issues that cannot be overcome with conventional bulk materials [33].

Nanomaterials can be found naturally, produced by chemical processes, or through engineering. They can be further tailored to perform various specialized functions [34], [35].

2.2 Properties of Nanomaterials

Materials at the nanoscale are influenced by the laws of quantum physics. Conversely, bulk-form materials follow the rules of classical physics. Due to the smallness of nanomaterials, their mass is extremely small, and gravitational forces become negligible. In the case of nanomaterials, electromagnetic forces are dominant in determining the behavior of atoms and molecules. For objects of very small mass, such as the electron, wavelike nature has a more pronounced effect. As a result, nanomaterials can demonstrate different physical and chemical properties to their bulk-form counterparts [36]. Some major characteristics of nanomaterials are discussed below:

2.2.1 Quantum Tunneling

Quantum tunneling is a fundamental quantum mechanical effect. In classical physics, a physical body can pass a barrier (potential barrier) only if it has enough energy to jump over it. Therefore, if the object has lower energy than that needed to jump over the energy barrier (the —obstacle), the probability of finding the object on the other side of the barrier is null. On the other hand, in quantum physics, a particle with energy less than that required to jump the barrier has a finite probability of being found on the other side of the barrier [37]. It is like the particle passes into a virtual tunnel through the barrier as seen in **Figure 2.1**. However, to cause a tunnel effect, the thickness of the barrier (i.e., energy potential) must be comparable to the wavelength of the particle which is observed only at the nanometer level. In other words, when a wave function/particle can propagate through a potential barrier, tunneling can occur on the nanoscale. Tunneling is also known as the penetration of an electron into an energy region that is classically forbidden. Quantum tunneling has a wide array of applications including scanning tunneling microscope [38] and the tunnel diode [39].

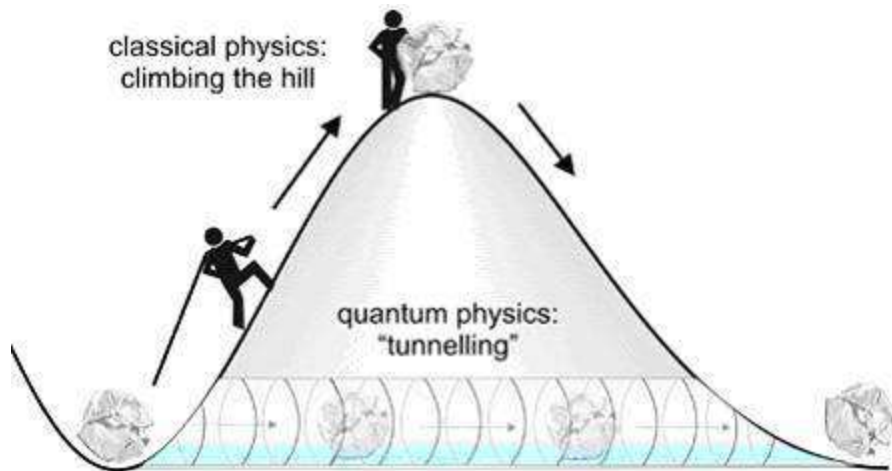


Figure 2.1: Schematic representation of tunneling [40].

2.2.2 Quantum Confinement

Using the electrical properties of materials quantum confinement can be explained. Based on electrical properties, there are three kinds of materials which are (1) conductors, (2) Semiconductors, and (3) insulators. The energy separation between the

valence band and the conduction band of a material is called band gap (E_g). Whether a material is a conductor, a semiconductor, or an insulator is determined by the filling capability of the conduction band with electrons and the energy of the band gap. In conducting materials like metals, the value of E_g is very small, as a result, the valence band and the conducting band overlap. Thermal energy is sufficient to influence electrons to move to the conduction band. The band gap of semiconductors is a few electron volts. When an applied voltage surpasses the band gap energy, the electron jumps to the conduction band from the valence band, thereby forming electron-hole pairs. Insulators have a large band gap that requires an enormous amount of voltage to overcome the threshold causing them not to conduct electricity. **(Figure 2.2)**

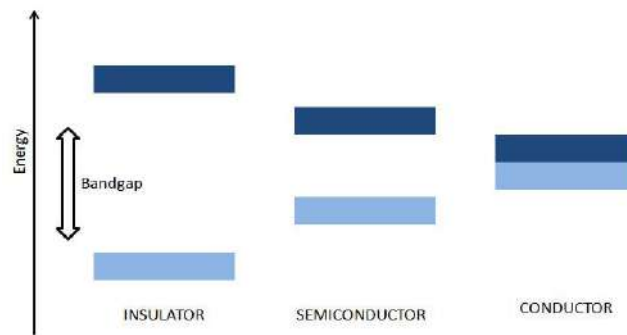


Figure 2.2: Band diagram of Insulator, semiconductor, and conductor [40].

In nanomaterials, the movement of electrons is restricted in space which is contrary to their behavior in bulk materials in which electrons are capable of moving freely. This phenomenon is known as Quantum confinement [41]. Quantum confinement is responsible for increasing the energy of the band gap as illustrated in **Figure 2.3**. As a result, more energy will be required to be absorbed by the band gap of the material.

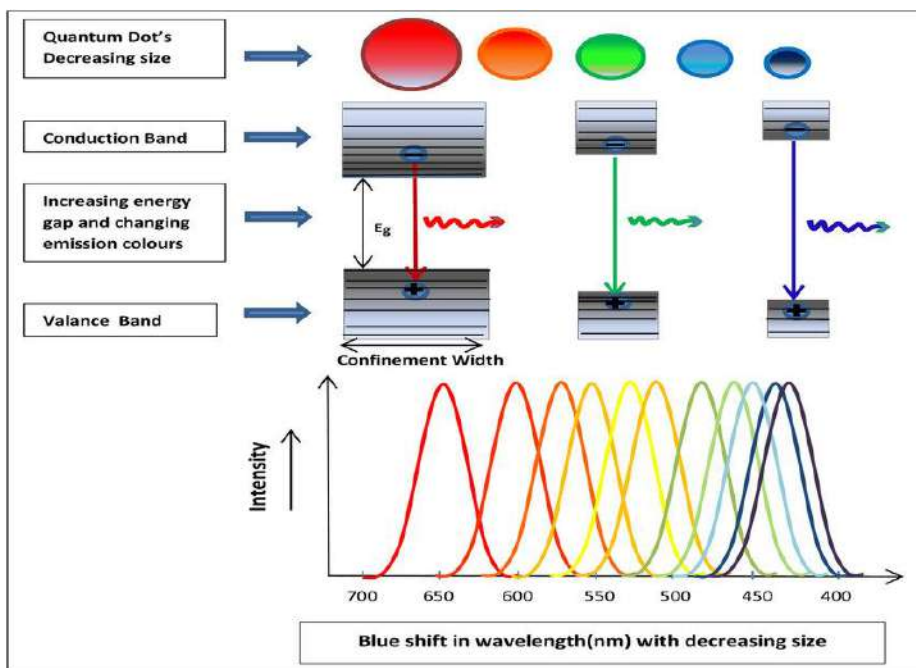


Figure 2.3: Illustration of quantum confinement effect [42].

At the nanoscale, the band overlap present in metals disappears and is transformed into a band gap. This is the reason why some metals become semiconductors as their size is reduced. The requirement of higher energy due to quantum confinement corresponds to a shorter wavelength (blue shift). The same blue shift will occur in the case of fluorescent light emitted from nanomaterials which have a shorter wavelength and higher energy. This phenomenon enables tuning of the optical absorption and emission properties of a nano-sized semiconductor over a range of wavelengths by controlling its crystallite size.

2.2.3 Optical Properties

The nanoparticles have discrete band levels which are separated with definite energy. In a QD, the presence of discrete energy levels widens the energy gap between the highest occupied electronic states and the lowest unoccupied states as compared to the bulk material. For this reason, the optical properties of the semiconductor nanoparticles are size-dependent [43]. For a smaller particle, higher energy is required for an electron to

get excited. As a result, shorter wavelengths of light are absorbed to cross a band gap of greater energy, i.e., a blue shift appears.

2.2.4 Surface Properties and Shape also Matters

It is a boundary between two phases, the material and the surrounding environment (liquid, solid, or gas), the term interface, rather than surface, is often used in the case of nanomaterials. If a bulk material is subdivided into an ensemble of individual nanomaterials, the total volume remains the same, but the collective surface area is greatly increased. As a result, the surface-to-volume ratio of the material is increased compared to that of the parent bulk material.

Nanomaterials possess a notable proportion of atoms existing at the surface. As a result, a profound effect is obtained on reactions that occur at the surface such as catalysis reactions, detection reactions, and reactions that, to be initiated, require the physical adsorption of certain species at the material's surface [44]. The fact that a larger fraction of the atoms present at the surface of a nanomaterial influences some physical properties such as the melting point (lower). Given the same volume, the extent of the surface area is depended on the shape of the material. For example, when a sphere and a cube have the same volume, the cube has a larger surface area than the sphere. For this reason, not only the size of a nanomaterial but also its shape is important in nanoscience [45].

2.3 Uses of Nanomaterials

Nanomaterials are the rapidly developing field of nanotechnology. Their unique size-dependent properties make these materials superior and indispensable. Therefore, they can be used for a range of structural and non-structural applications. As nanomaterials possess advantageous, exclusive physical, chemical, and mechanical properties, nanotechnology and nanomaterials can be applied in electronics, energy production, aerospace, biomedicine, textile, healthcare, and cosmetics industries. Self-cleaning coated surfaces, air purification with ions, wastewater purification with nanobubbles, or

nanofiltration systems for heavy metals are some of its environmentally-friendly applications [45]–[48]. Nanocatalysts are also used to make chemical reactions more efficient and less polluting.

2.4 Electronic and Crystal Structures of TiO₂

TiO₂ has three polymorphs which are - anatase, rutile, and brookite. Among these three crystal structures, only anatase shows higher photocatalytic activities. Although rutile is the stable phase in general, anatase shows good stability in the nanoscale [49]. Brookite is rarely considered a photocatalyst due to the difficulties associated with its synthesis. Anatase as a semiconductor, has an indirect band gap, whereas rutile and brookite have direct band gaps [9]. Because of its indirect band gap, anatase shows a longer lifetime of photogenerated electrons and holes than brookite and rutile. In anatase, the direct transition of photogenerated electrons from the conduction band to the valence band is impossible due to this indirect band gap.

Again, the average effective mass of photogenerated electrons and holes in anatase is smaller than that of rutile and brookite. As a result, the transfer rate of the holes and electrons in anatase is the fastest among the three materials. For this reason, the photoexcited charge carriers of anatase migrate more easily and transfer to the surface from its interior to participate in photocatalytic reactions [9].

The most common form of TiO₂ is the densely packed rutile phase. As seen in **Figure 2.4**, the anatase phase has an open tetragonal crystal structure which makes it highly photocatalytic. Rutile also has tetragonal structure. The brookite phase is orthorhombic and extremely rare. Among these phases, anatase TiO₂ draws the most attention because of its higher reactivity and chemical stability.

Due to its higher reactivity, anatase TiO₂ has been the focus of most of the investigations regarding semiconductor-based photocatalysis [49]–[51]. In the presence of ultraviolet light ($\lambda < 390$ nm), photocatalytic activity on the TiO₂ surface is triggered by photogenerated electrons and holes. Its energy exceeds the band gap of 3.2 eV in the anatase crystalline phase. This process requires exposure to sunlight containing UV light

which is only about 3%. Such condition limits the range of the applications of this technology. Only those photocatalysts that can yield high reactivity under visible light ($\lambda > \sim 390$ nm), will allow the use of the main spectrum of sunlight to be utilized for useful purposes.

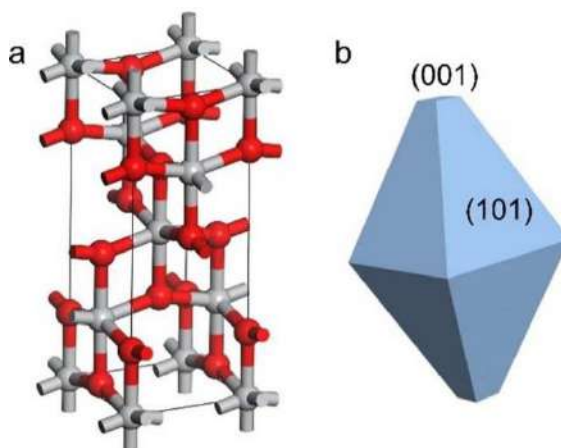


Figure 2.4: (a) Crystal Structure of anatase where Ti atoms are grey and O atoms red. (b) Equilibrium crystal shape of anatase TiO_2 [52].

The electronic structure of TiO_2 is the basis for designing the band gap modification for visible-light sensitization. Several ab initio calculations were carried out to study the electronic structure of TiO_2 [53]–[55]. A fundamental characteristic of the electronic structure for anatase TiO_2 is shown in a molecular orbital bonding diagram presented in **Figure 2.5** [55]. At the top of the valence bands (VBM), there is the nonbonding O p_π orbital (out of the Ti_3O cluster plane) and at the bottom of the conduction bands (CBM) are the nonbonding d_{xy} states. A similar feature is found in rutile where it is less significant than in anatase [56]. Each octahedron in rutile shares corners with eight neighbors, and edges with two other neighbors, resulting in a linear chain. On the other hand, a zigzag chain with a screw axis is created when in anatase each octahedron shares corners with four neighbors and edges with four other neighbors. Therefore, anatase is less dense than rutile. Anatase also has a large metal–metal distance of 5.35 Å. As a result, the Ti d_{xy} orbitals at CBM are relatively isolated, while the t_{2g} orbitals at CBM in rutile provide the metal-metal interaction with a smaller distance of 2.96 Å. Thus, the bandwidth of anatase is smaller than that of rutile. Anatase

has a slightly wide band gap of 3.2 eV as compared to 3.0 eV for rutile [10]. Generally, the anatase to rutile phase transition occurs in a wide temperature range of 600°C – 1100°C [57]. That's why during anatase synthesis, less than 600°C annealing temperature is maintained to get more anatase structure.

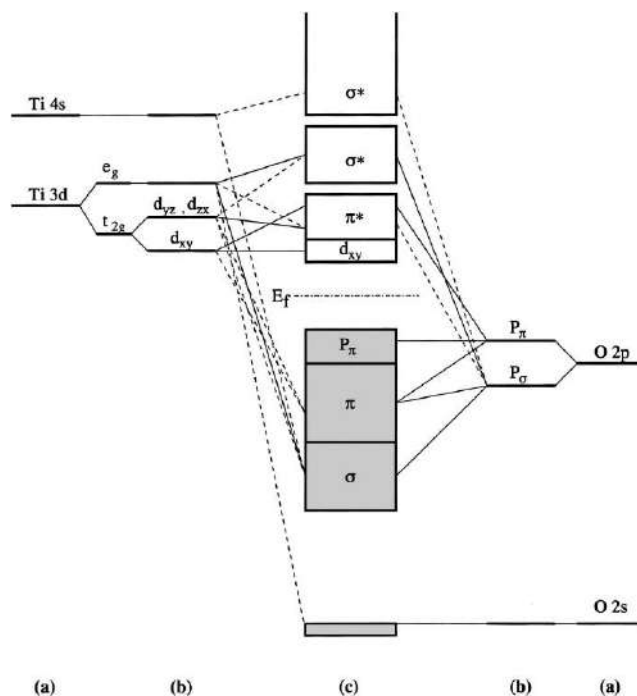


Figure 2.5: Molecular-orbital bonding structure for anatase TiO₂:(a) Atomic levels (b) Crystal-field split levels (c) Final interaction states. The thin-solid and dashed lines represent large and small contributions, respectively [55].

2.5 Modification Technique of TiO₂

As regular TiO₂ is not sufficiently photo-active in the presence of visible light, its band gap must be modified so that the major part of solar radiation and interior lighting can be properly utilized. The following three techniques have been proposed to make TiO₂ sensitive to visible light [10] -

- (i) A lower shift of conduction band minimum (CBM)
- (ii) A higher shift of valence band maximum (VBM)
- (iii) Introduction of impurity states in the band gap

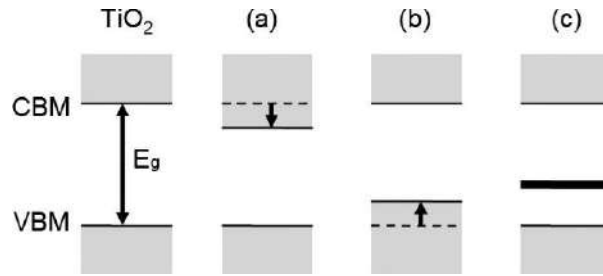


Figure 2.6: Three schemes for band gap modifications for visible-light sensitization: (a) Lower shift of CBM (b) A higher shift of VBM (c) Introduction of impurity states [10].

Figure 2.6 is a graphical representation of the techniques proposed for band gap modification. These techniques are focused on basically one thing – to shorten the band gap of TiO₂ nanoparticles.

Asashi, *et al.* [58] found N 2p state creates hybrids with O 2p states in anatase TiO₂ doped with nitrogen. It is because of the fact that their energies are very close, and thus the band gap of N-TiO₂ is narrowed which enables it to absorb visible light. Irie, *et al.* [59] stated that TiO₂ oxygen sites substituted by nitrogen atom form isolated impurity energy levels above the valence band. Illumination with visible light only excites electrons in the impurity energy level, although irradiation with UV light excites electrons in both the VB and the impurity energy levels. Ihara, *et al.* [60] concluded that oxygen-deficient sites can also help the photocatalytic mechanism. These sites formed in the grain boundaries are important to emerge vis-activity and nitrogen-doped in parts of oxygen-deficient sites is important as a blocker for re-oxidation.

Such type of modification mechanism of anatase doped with nonmetals was also analyzed by Zhao *et al.* [61]. They concluded that TiO₂ doped with substitutional nitrogen has shallow acceptor states above the valence state after investigation. However, TiO₂ doped with interstitial nitrogen has isolated impurity states in the middle

of the band gap. It was found that these impurity energy levels are mainly hybridized by N 2p states and O 2p states.

Absorption of photons having energy ($h\nu_1$) equal to or greater than the band gap of anatase (3.3 eV) triggers photocatalysis. As a result, an electron-hole pair is produced on the surface of the TiO_2 nanoparticle as shown in **Figure 2.7**. A positive hole is created in the valence band when an electron migrates to the conduction band from it. Several things can happen with the excited-state electrons and holes: they can recombine and dissipate the input energy as heat, get trapped in metastable surface states, or react with electron donors and with electron acceptors adsorbed on the solid surface or within the surrounding electrical double layer of the charged particles. These holes produce hydroxyl radicals with high redox oxidizing potential. If conditions are met, the holes, $\cdot\text{OH}$ radicals, O_2^- , H_2O_2 , and O_2 itself can play important roles in the photocatalytic reactions [62].

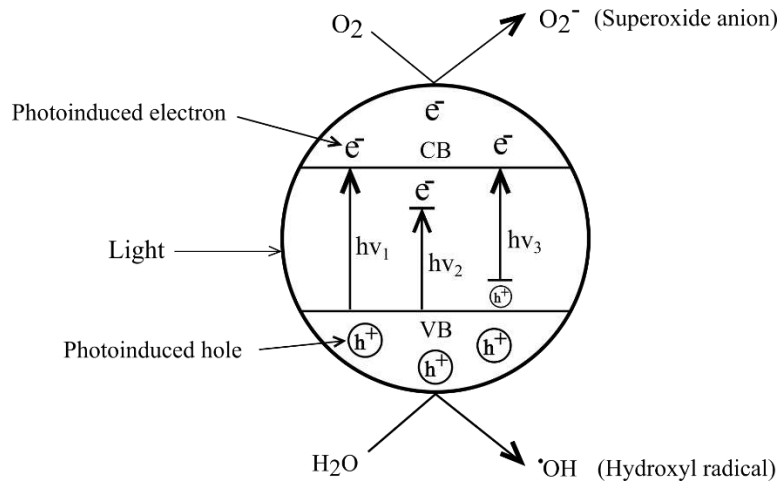


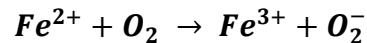
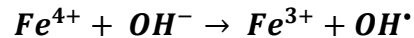
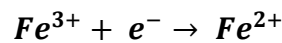
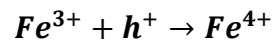
Figure 2.7: Mechanism of TiO_2 photocatalysis. $h\nu_1$: pure TiO_2 , $h\nu_2$: metal-doped TiO_2 , $h\nu_3$: nonmetal-doped TiO_2 [63].

The Photoactivity of metal-doped TiO_2 under visible light can be explained by a new energy level produced in the band gap of TiO_2 by dispersing metallic nanoparticles in the TiO_2 matrix. By the action of photons having energy $h\nu_2$, electrons from the defect state are excited to the conduction band. Another goal for using transition metal doping

is to trap the electrons well so that electron-hole recombination can be avoided. Inhibition of this recombination process results in increased photoactivity.

2.6 Photocatalytic Activity of Fe-doped TiO₂

The doping of Fe in Nano-TiO₂ causes the incorporation of Fe³⁺ ions into the crystal lattice of TiO₂. As a result, the band gap decreases and a red shift in the light absorption occurs. This enables the photocatalyst to be activated under visible light illumination. Moreover, the energy level of Fe³⁺/Fe⁴⁺ is above the valence band energy and that of Fe³⁺/Fe²⁺ is below the conduction band energy of TiO₂ [64]. Therefore, Fe³⁺ reacts with both holes and electrons and forms Fe⁴⁺ or Fe²⁺ traps [65]. On the other hand, Fe²⁺ and Fe⁴⁺ are less stable than Fe³⁺. That's why Fe²⁺ and Fe⁴⁺ eventually revert to the Fe³⁺ state upon their release of the electron and hole at the surface of the photocatalyst initiating the photocatalytic reactions [66], [67]. Thus after light absorption by Fe-doped TiO₂, the photo-generated electrons and holes are created, and concomitantly hydroxyl and superoxide radicals are generated as follows [15], [68]. **(Figure 2.8)**



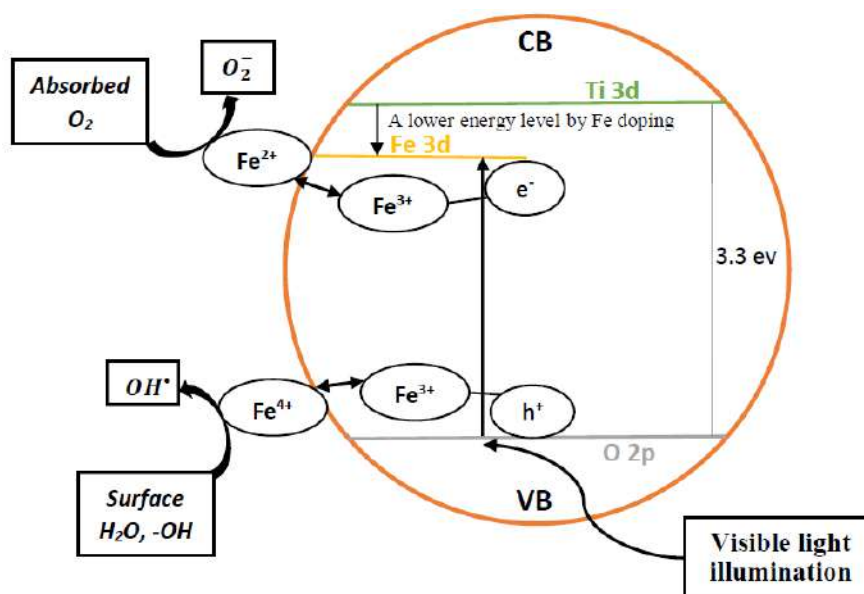


Figure 2.8: Schematic representation of mechanism involved in photocatalytic activity of Fe-doped TiO₂ [63].

2.7 Notable Scholarly Works Regarding Fe-doped TiO₂

Visible light-sensitive Fe-doped TiO₂ photocatalyst was successfully prepared by *Moradi et al.* by sol-gel method using titanium isopropoxide (TTIP) as the precursor and ferric nitrate nonahydrate (Fe(NO₃)₃·9H₂O) as doping source [15]. The crystallinity of synthesized anatase decreased gradually with the increase in the Fe doping content. The increase in the doping content decreased the band gap energy from 3.3 eV to 2.9 eV and particle size from 3 nm to 5 nm. They observed a contaminating amorphous layer of iron oxide on the surface of catalyst particles. Treating with an HCl solution the amorphous layer was successfully removed. It was observed that after removing the amorphous layer the photocatalytic activity increased significantly from 24% to 98% under visible light illumination.

Fe-doped TiO₂ powders were prepared by *Marami et al.* by the sol-gel method using titanium(IV) isopropoxide (TTIP) as the precursor, ethanol as solvent, ethylene

glycol (EG) as stabilizer and $\text{FeSO}_4 \cdot 7\text{H}_2\text{O}$ as doping source [69]. The particle size of Fe-doped TiO_2 was in the range of 18–39 nm. The lowest crystallite size was obtained for 4 mol% of Fe. Both anatase and rutile phases were found and with various molar concentrations of Fe dopant, their ratio changed. Crystallite size decreases with the increase of Fe doping as demonstrated by XRD. At about 2.6 eV for 4 mol % Fe-doped TiO_2 , the optimal band gap was achieved. The photocatalytic activity was increased by the Fe^{3+} ions by the separation of photogenerated charges, significantly affecting the material efficiency as a photocatalyst for solar energy conversion.

Gullapelli Sadanandam et al produced Fe-doped TiO_2 with various levels of Fe (0.5, 1, 2, 3, and 5 wt. %) via impregnation [70]. The Fe-doped TiO_2 catalysts were further modified with g- C_3N_4 (graphitic carbon nitrides). The photoresponse of titania expanded into the visible region by the fine dispersed Fe^{3+} and g- C_3N_4 . The catalyst's photocatalytic activity was tested by hydrogen production from pure water splitting. By coupling g- C_3N_4 with the above Fe-doped TiO_2 , the hydrogen formation rate from solar light-induced photocatalysis can be increased significantly. High photoactivity and stability are particularly shown by the 1 wt. % Fe-modified TiO_2 with the g- C_3N_4 composite for hydrogen production by solar irradiation. The stable hydrogen evolution in the case of 1 wt.% Fe-doped TiO_2 with g- C_3N_4 was found to be 17 times higher than in the case of unmodified TiO_2 . A near-doubling of the rate was seen when g- C_3N_4 modification on Fe-doped TiO_2 was carried out compared with bare Fe-doped TiO_2 catalysts, which can be attributed to synergetic effects occurring among the components Fe^{3+} , g- C_3N_4 , and TiO_2 .

Kim et al. successfully prepared visible light active Fe–N– TiO_2 photocatalyst by sonochemical method [71]. The synthesized co-doped TiO_2 nanopowder was of anatase phase and possessed a specific surface area of $75 \text{ m}^2\text{g}^{-1}$. The nitrogen and iron dopants are possibly placed into the TiO_2 lattice, replacing some Ti^{4+} and O_2^- respectively which enabled the band gap to be sensitized by the visible region of light. The absorption area of the doped TiO_2 has been red-shifted towards 600 nm. The doped nanoparticles

exhibited good photocatalytic activity on the degradation of indigo carmine dye (ICD) under solar radiation. The incorporation of N and Fe caused the diminishing of electron-hole recombination and improved the photocatalytic activity under simulated solar light.

Ping Yu et al. synthesized N, Fe doped TiO₂ photocatalyst by sol-gel method [72]. The prepared catalyst was characterized by X-ray diffraction (XRD), Fourier transform infrared (FT-IR), and ultraviolet and visible spectroscopy (UV-vis). The analyses showed that the N, Fe doped TiO₂ had the anatase structure. The absorption edge of the photocatalyst shifted to a longer wavelength and the degradation of methylene blue (MB) under Xe-lamp (350 W) was much more active than in the cases of un-doped TiO₂, N-doped TiO₂, and Fe-doped TiO₂ as seen in **Figure 2.9**.

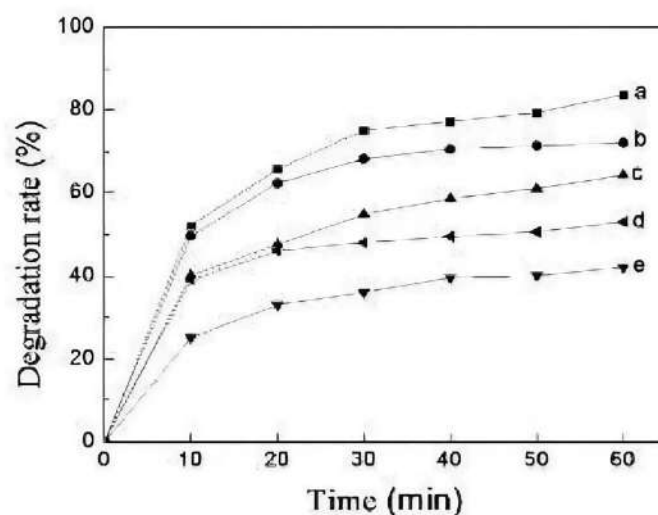


Figure 2.9: Photocatalytic degradation of MB for samples of (a) N-Fe-TiO₂, (b) Fe-TiO₂, (c) N-TiO₂, (d) P-25, (e) TiO₂ [72].

Ionela et al. found that the physical properties of the polyester fabrics treated with nitrogen and iron co-doped TiO₂ nanoparticles prepared by the hydrothermal method were not significantly modified [73]. However, the use of a polyacrylic binder allowed the deposition of a higher number of nanoparticles on the textile surface which improved the photo-discoloration efficiency under visible light radiation. Their findings further reported the biocompatibility on human skin cells of PES (polyester) fabrics

modified with photocatalytic TiO₂-1% Fe-N nanoparticles which could be further used as novel materials for biomedical applications, such as disposable operatory fields, hospital sheets, medical robes and wound dressing for preventing patients' accidental contamination with microorganisms from the hospital environment.

Ramalingam et al. synthesized N and Fe-doped TiO₂ nanoparticles by a one-step template-free hydrothermal method and electro-deposition technique [74]. The XRD analysis of all the catalysts showed the presence of the crystalline anatase phase with a crystallite size in the range of 20–25 nm for the N-doped TiO₂ nanoparticles. On the other hand, the average particle size for the Fe-N-TiO₂ sample was found to be 12 nm. Very fine rectangle-shaped nanoparticles were formed in the case of the Fe-N-TiO₂ photocatalyst. Fe-N-doped TiO₂ catalysts demonstrated the best result for photoelectrochemical and visible light-activated catalysis. For the NT2 (0.5N:1Ti) photo anode, the enhanced activity with a photocurrent of 0.25 mA/cm² at 1V vs RHE was obtained. The doped TiO₂ can be utilized in water-splitting reactions for hydrogen production.

Larumbe et al. prepared Fe, N doped TiO₂ nanoparticles by sol-gel method and made a comparative study with undoped TiO₂ samples [75]. Nanoparticles of monophasic anatase structure with an average diameter of around 4-6.5 nm were obtained under calcination at 300°C (1h). Both doping elements induced a red-shift of the absorption curves due to the introduction of a new intragap energy level. It resulted in an enhancement of the photocatalytic activity for the nitrogen-doped samples. At low temperatures, magnetic measurements evidenced an antiferromagnetic nature in Fe-doped samples correlated to the homogeneous distribution of Fe³⁺ in the nanoparticles. This resulted in the deterioration of the photocatalytic activity due to the reduction of the electron/hole pairs that could reach the surface of the nanoparticles. A weak ferromagnetic behavior was detected at room temperature in the case of nitrogen-doped samples which is related to the formation of oxygen vacancies. The photocatalytic

activity is reduced with the increase of the nitrogen concentration as these oxygen vacancies act as recombination centers.

Ohwaki et al. reported improvements in the photocatalytic activities of N-TiO₂ upon modification with Cu or Fe compounds to obtain visible-light sensitive photocatalysts [76]. X-ray absorption fine structure (XAFS) has been used to investigate the valence state of Cu on the modified N-TiO₂ and the results indicated that it was in its hydroxide form. The mechanism by which the photocatalytic activity is enhanced has been discussed based on an increased number of active oxidative species.

Li et al. reported that the N, Fe co-doped TiO₂ shows higher photocatalytic efficiency than pure TiO₂, N-TiO₂, Fe-TiO₂, and P-25 (Degussa) [77]. Most of the samples presented high photocatalytic activity under natural light. In 60 minutes, approximately 96.4% methyl orange (MO) was degraded. The high photocatalytic activity may be attributed to the small diameter of 17 nm of N-Fe-TiO₂ and the high specific surface area of about 201 m²/g. The increase of the photogenerated electrons would be facilitated by a smaller particle size and a larger specific surface area. Also, the anatase phase of the samples possessed the best photocatalytic activity. The tailored band gap was another important reason for the best photocatalytic activity of the N-Fe-TiO₂.

Zhang et al. prepared Fe–N co-doped mesoporous TiO₂ photocatalyst via the fast sol-gel method by introducing PAM (polyacrylamide) and PEG (polyethylene glycol) as the bi-templates [78]. It had a high surface area, well-order mesoporous structure, and high visible light photocatalytic activity. It was observed that the sol-gel reaction velocity was accelerated and the reaction time was reduced to several hours. This could be attributed to templates produced by the intermolecular hydrogen bond and the polymerization crosslink of the hydrolysates of Ti alkoxides. It has been speculated that the fast sol-gel method may have more potential for practical application than the

conventional sol-gel method, because of its fast preparation process and lower cost for templates.

Zhang et al. suggested that undoped TiO₂ had no photocatalytic activity under visible light irradiation [63]. TiO₂ co-doped with N and Fe broadened the range of response to visible light, providing a technique to purify outdoor air. Co-doping with N and Fe also strengthened the photocatalytic activity of TiO₂ under UV and visible light which was demonstrated by the decomposition of NH₃. However, high calcination temperature had a negative effect on the photocatalytic activity of TiO₂. The addition of N and Fe to TiO₂ lessened this negative effect of calcination temperature on TiO₂. The average particle size of co-doped anatase samples was 20 nm. They found that the traps of the N-2p, Fe-3d, and Ti-3d orbitals inhibited the recombination of photogenerated hole–electron pairs, which improved the photocatalytic quantum efficiency of TiO₂.

Kaur et al. synthesized nanocrystalline undoped, N-doped, and N, Fe co-doped TiO₂ by sol-gel method for the photocatalytic degradation of Reactive Blue 4 dye under visible light [79]. They found that the N, Fe co-doped TiO₂ exhibited the best photocatalytic activity. To solve the problem of separation of N, Fe co-doped TiO₂ photocatalyst, magnetically separable γ -Fe₂O₃/N, Fe co-doped TiO₂ heterojunction was fabricated. This caused to exhibit higher photoactivity with 100% dye degradation as compared to 85% with N, Fe co-doped TiO₂ as seen in **Figure 2.10**.

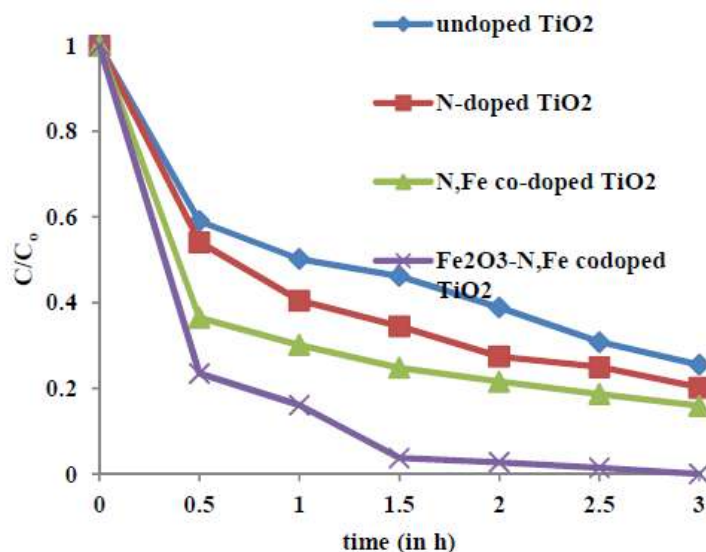


Figure 2.10: Photocatalytic degradation of RB 4 dye with synthesized catalysts; $C_0=10$ ppm, catalyst amount= 0.24 gm/200 ml [79].

The enhanced electron-hole transfer in γ -Fe₂O₃/N, Fe co-doped TiO₂ heterojunction, low electron-hole recombination rate, the existence of pure anatase phase, and a narrow band gap of 1.5eV are responsible for this behavior. Good repeatability of photoactivity was also exhibited by the recycled γ -Fe₂O₃/N, Fe co-doped TiO₂.

2.8 Applications of TiO₂ Nanoparticles

The potential applications of TiO₂ nanoparticles are numerous and are coming to light only recently. Although the following applications have been suggested and experimented with TiO₂ nanoparticles in general, Fe-doped TiO₂ can be applied to obtain better results when photocatalysis is involved.

Water Treatment

Decontamination of water from organic pollutants during agricultural production has led to research on developing methods that lower the consumption of chemical reagents [80]. The photocatalytic decomposition of organic pollutants in water is of particular interest and has received significant attention from scientists [81], [82]. By far, TiO₂ is

the most popular semiconductor that is used in photocatalytic processes. Large-sized TiO₂ semiconductors are stoichiometric and exhibit poor photocatalytic activity, however, nano-TiO₂ crystallites (typical size <50 nm) have the desired electronic properties for application in photocatalysis [83]. Reactive species can be formed on the surface of a nano-TiO₂ photocatalyst that is exposed to UV radiation through this photocatalysis process. In most cases, the complete degradation and mineralization of a large variety of organic contaminants can be achieved.

The main obstacle that has limited the practical application of nano-TiO₂ in water purification is either a relatively low process rate or a limited efficiency for the use of irradiated energy [84], [85]. The exploitation of low-cost radiation such as solar energy can be a solution to this problem [86], [87]. As the intensity of ultraviolet radiation in the solar spectrum is very limited, the use of metals or metal oxide doping to extend the TiO₂ nanoparticles' sensitivity to visible light is currently a widely suggested option for solving the problem. For instance, it was observed that the degradation rate of phenol is significantly enhanced by the addition of fluoride to TiO₂ [88]. Vione et al. reported similar findings about fluoride-doped TiO₂ [80]. Bessekhoud et al. reported that alkaline-doped TiO₂ at low concentrations could be a promising material to degrade organic pollutants and the best results were obtained for 5% Li-doped TiO₂ that was prepared using the impregnation technique [83]. Brezová et al. reported that the photoactivity of TiO₂ can be improved by the doping of metals, such as Li⁺, Zn²⁺, Cd²⁺, Pt⁰, Ce³⁺, Mn²⁺, Al³⁺, and Fe³⁺ through sol-gel technique [89].

Ling et al. prepared TiO₂ nanoparticles (with diameters of 10–23 nm) that showed good photocatalytic activity [90]. They reported that the initial degradation rate of phenol by the action of TiO₂ nanocatalyst was 6 times higher than what was achieved with H₂O₂. Moreover, the addition of H₂O₂ to TiO₂ can increase the initial concentration of hydroxyl radicals and accelerate the degradation rate.

Hao et al. developed a TiO₂/WO₃/GO nanocomposite (via a hydrothermal synthesis), which displayed excellent photocatalytic activity for the degradation of

bisphenol A [91]. The photogenerated electrons on TiO₂ have a strong reducing capacity to remove pollutants including Cd (II), Hg (II), As (V), and Cr (VI) from water. Dusadee et al. fabricated a titania-decorated reduced graphene oxide (TiO₂/rGO) nanocomposite via a hydrothermal process that can be used to degrade organic pollutants [92]. Studies on reducing the Cr⁶⁺ ion toxicity using the titanium dioxide x/rGO numerical control have demonstrated that photocatalytic reduction of toxic Cr⁶⁺ generally increases with the increase in x. The combination of photoexcited electrons and holes decreases which leads to an increased duration of photocatalytic activity, since rGO accelerates electron transport [92]. Many pollutant degradation processes such as the reduction of nitrate, the degradation of acid fuchsin, the decomposition of acetaldehyde, and the dechlorination of CCl₄ have been facilitated by TiO₂ [93], [94].

Air Treatment

Industrial development throughout the world has put a negative effect on our environment. Air pollution endangers the health of all species that live in this world and therefore, new techniques are being developed to reduce harmful airborne emissions. Highly efficient oxidation and reduction during photocatalysis is considered to be an effective method to degrade inorganic and organic air pollutants [95], [96]. Kakeru et al. prepared TiO₂ nanoparticles with palladium sub-nanoclusters (<1 nm) using the flame aerosol technique which under sunlight, can remove NO_x at approximately 3 to 7 times the rate of commercial TiO₂ (P-25, Evonik) (without Pd) [97].

Natércia et al. used a hydrothermal method to prepare a new composite material of TiO₂ (P-25) and N-doped carbon quantum dots (P-25/NCQD), which was applied as the photo-oxidation catalyst of NO under the presence of ultraviolet and visible light [98]. The conversion rate of the P-25/NCQD composite material (27.0%) was more than twice that of P-25 (10%) without modification and the selectivity in visible light increased from 37.4% to 49.3%. Also, the photocatalytic performance of the composite material in the UV region was better than that of P-25.

Zeng et al. have proposed an H₂ reduction strategy to produce H-TiO₂ materials (with enhanced oxygen vacancy concentrations and distributions) that can promote

formaldehyde decomposition in the dark [99]. Research of TiO₂-based photocatalysts has also been carried out to facilitate the removal of acetone [100], benzene [101], phenol [102], tetrachloroethylene [103], etc. from the atmosphere.

Pesticide Degradation

Repeated use of pesticides results in excessive chemical residues in the environment and biota. Scientists have made efforts to develop methods that can remove residual pesticides and destroy biorecalcitrant organic contaminants [104]. Semiconductor photocatalysis has attracted significant attention among the scientific community as it is a promising approach to remedy the pesticide residue problem [105], [106]. Pesticides are decomposed by the action of TiO₂ photocatalysts in the presence of a UV light source. Electron-hole pairs are produced when TiO₂ is irradiated with photons whose energy is equal to or greater than its band gap energy ($E_g = 3.2$ eV). These holes react with H₂O or OH⁻ that are adsorbed on the semiconductor surface to produce ·OH radicals in an aqueous system, which are the strongest oxidants in this process [107]–[109]. These radicals react with pesticides that are adsorbed on the surface and decompose them. The pesticides are degraded into various forms like H₂O, CO₂, and other biologically degradable and less toxic substances that are without secondary pollution. It was reported that the TiO₂ photocatalyst is effective in degrading the phosphamidon insecticide [110]. Lhomme et al. observed and reported the photocatalytic degradation of chlortoluron and cyproconazole pesticides on TiO₂-coated media, and the process was found to be effective [111]. This photocatalytic degradation process of pesticides is mainly based on the in-situ generation of highly reactive ·OH radicals, which are capable of converting pesticide molecules into relatively harmless end products. However, the high rate of electron-hole recombination, wide band gap, etc. are the limitations for the wide application of TiO₂ semiconductors for pesticide photocatalytic degradation [112], [113]. The major criteria for the increase of photocatalytic efficiency for pesticide degradation are the minimization of the electron-hole recombination and efficient visible light excitation. To overcome these limitations,

many modification strategies have been applied to TiO₂ nanomaterials such as doping with metal and/or non-metal.

Self-cleaning Objects

Daily atmospheric deposits of dirt, soot, and other pollutants released by various sources including vehicles, industries, forest fires, etc. lead to a constant need of cleaning buildings. Also, the growth of various microorganisms disfigures and corrodes infrastructures, causing mechanical weakness and even dilapidation. One approach to get rid of this problem is to cover the construction exterior using materials that contain nano photocatalysts. Commercial surfaces with self-cleaning properties are usually made of thin TiO₂ layers whose photo-induced catalytic performances are well-known nowadays [114]. It is important to note that TiO₂-coated surfaces can show hydrophilic characteristics under illumination and hydrophobic characteristic in the absence of light. This superhydrophobic character is due to the roughness induced by the nanoparticles, preventing them from wetting or soiling. This phenomenon is inspired by nature and was observed for the first time in *Nelumbo nucifera* leaves, widely known as the "Lotus Effect" [115].

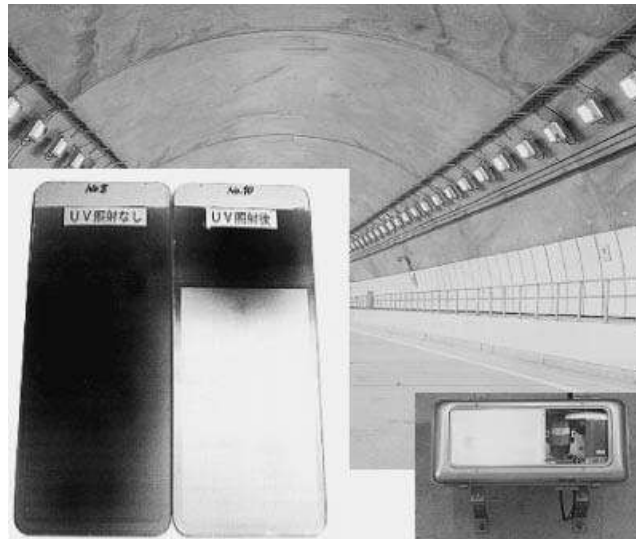


Figure 2.11: Glass covers on highway tunnel lighting fixtures darkened by automobile exhaust without TiO₂ and maintained clean with TiO₂ [23].

The self-cleaning properties of TiO₂ nanoparticles (NPs) have not remained at the research stage only; they have been employed in practical applications by many companies. For example, Activ™ glass developed by Pilkington is one of the most successful commercial self-cleaning products which are being used in different buildings around the world [116]. The hydrophilicity of nanoparticles has been used in self-cleaning cover glass for tunnel light in Japan. Yellow light-emitting sodium lamps are used for lighting in most tunnels, and the decrease in light intensity due to film formation with exhaust compounds is one of the most serious problems. At the position of its cover glass, a high-pressure sodium lamp also emits UV light of about 3mW/cm². This UV light is sufficient to keep the surface clean when the cover glass is coated with the TiO₂ photocatalyst, although not considered in the original purpose of the lighting (**Figure 2.11**) [117].

Another photo-induced superhydrophilicity-based technology being used widely is Hydrotect™, introduced by the Japanese company TOTO Ltd. [118]. Self-cleaning windows and tiles are widely used in Japan and other countries are also starting to utilize this new technology. Glass and cement containing TiO₂ NPs have also been used on the surface of the National Opera Hall in China, in “Dives in Misericordia” Church in Rome, and on the roof of Dubai Sports City’s cricket stadium [119].

Interior

Researchers have been trying to create interiors with functions that can eliminate odors and volatile organic compounds (VOCs) in indoor air and prevent bacterial or viral infection for a long time. Many studies on the elimination of odors and VOCs [120], [121] and the prevention of bacterial and viral infections using photocatalytic oxidation in the presence of light have been carried out [122]. N-doped TiO₂ photocatalysts have been successfully applied to decrease odors and VOCs in indoor air. To secure the interior, N-doped TiO₂ coating solutions are used to maintain coatings that provide antifouling, deodorizing, antibacterial, and antiviral protection. Moreover, they are also

used in window shades, artificial flowers, Japanese paper, furniture made with artificial leather, and wallpaper.

Hydrogen Generation

Mankind is facing an unprecedented crisis with the ever-increasing population and its huge energy demand. The photogenerated electrons on the TiO₂ surface have a strong reducing capacity, enabling the generation of hydrogen from the photocatalytic splitting of water. Moreover, its potential as a truly clean energy source has received considerable attention, since hydrogen combustion produces only water and no harmful emissions. Photocatalytic hydrogen production is based on two essential elements: a semiconductor that absorbs the light to generate electron-hole pairs, and a metal that acts as an electron trapper or a co-catalyst [123]. Among all the potential semiconductors for photocatalysis that have been explored so far, TiO₂ remains the most suitable material for hydrogen production, owing to its intrinsic properties [124].

Zou et al. reported a self-modified TiO₂ material with paramagnetic oxygen vacancies that can be used to produce hydrogen [125]. They chose a porous amorphous TiO₂ material as a precursor that possessed a high surface area of 543 m²g⁻¹ for the synthesis of V_o-TiO₂ (V_o: denotes a paramagnetic oxygen vacancy). To obtain the V_o-TiO₂ material, the precursor was calcined in the presence of imidazole and hydrochloric acid at an elevated temperature in the air. The H₂ production rate was approximately 115 μmol h⁻¹g⁻¹ with the V_o-TiO₂ sample (for H₂ evolution from water) which used methanol as a sacrificial reagent under visible light (≥400 nm) at room temperature, which is substantially higher than that achieved with V_o-Ti³⁺-TiO₂ (32 μmol h⁻¹g⁻¹).

Zhou et al. introduced an ordered mesoporous black TiO₂ material that utilized a thermally stable and mesoporous TiO₂ with a high surface area as the hydrogenation precursor for treatment at 500°C [126]. The samples possessed a relatively high surface area of 124 m²g⁻¹ and exhibited a photo response that extended from ultraviolet to visible light. In the presence of solar radiation, the ordered mesoporous black TiO₂ material

exhibits a high hydrogen production rate ($136.2 \mu\text{mol h}^{-1}$), which is almost twice as high as that of pristine mesoporous TiO_2 ($76.6 \mu\text{mol h}^{-1}$).

A covalently bonded oxidized graphitic $\text{C}_3\text{N}_4/\text{TiO}_2$ heterostructure was made by Zhong et al. that markedly increased the visible light photocatalytic activity for H_2 evolution by nearly a factor of approximately 6.1 compared to a simple physical mixture of TiO_2 nanosheets and O-g- C_3N_4 [127].

CO₂ Reduction

The photogenerated electrons on TiO_2 are capable of generating valuable solar energy fuels such as CH_4 , HCO_2H , CH_2O , CH_3OH , etc. in addition to reducing water into hydrogen, which can alleviate the problems associated with the production of greenhouse gases from the combustion of fossil fuels. Cu-doped TiO_2 was prepared by Slamet et al. through an improved impregnation method for photocatalytic CO_2 reduction [128]. It was observed that Cu doping can greatly enhance the photocatalytic performance of TiO_2 with respect to CO_2 reduction. Liu et al. prepared copper-loaded titania photocatalysts via a one-pot, sol-gel synthesis method and found that it consisted of highly dispersed copper [129]. A strong volcano dependence on Cu loading was observed by CO_2 photoreduction, which was responsible for the transition from 2-dimensional CuOx nanostructures to 3-dimensional crystallites and optimum CH_4 production was observed for 0.03 wt.% Cu/TiO_2 .

Solar Batteries

For better performance, TiO_2 can also be applied to dye-sensitized solar cells, Li-ion batteries, Na-ion batteries, and supercapacitors. Electric energy can be obtained through charge transport since semiconductors absorb photons to produce photonic carriers, and the photonic carriers move and separate at the same time. A spring-like $\text{Ti}@\text{TiO}_2$ nanowire array wire was synthesized by Liu et al. that could be utilized as a photoanode in dye-sensitized solar cells. A conversion efficiency of more than 95.95% was exhibited by this configuration [130].

The use of anatase TiO₂ nanotubes on rutile TiO₂ nanorod arrays as photoanodes in quantum dot-sensitized solar cells was reported by another study indicating an impressive solar energy conversion efficiency of approximately 1.04%. Compared with solar cells using the original TiO₂ nanorod array photoanodes, this is almost 2.7 times higher [131]. Chen et al. prepared a C@TiO₂ nanocomposite as the anode material for lithium-ion batteries which utilized the esterification of ethylene glycol with acetic acid in the presence of potassium chloride. Li-ion batteries utilizing this technique exhibited excellent performance and specific capacity (237 mA h⁻¹g⁻¹), and a coulomb efficiency (CE) of approximately 100% after 100 cycles [132].

Su et al. utilized a template approach to synthesize anatase TiO₂ as the anode in Na-ion batteries; this resulted in better battery performance in comparison to that achieved when amorphous and rutile TiO₂ was used as the anode material [133]. Anatase titanium dioxide produced the highest capacity compared to other crystalline phases of titanium dioxide, 295 mAh⁻¹g⁻¹, in the second cycle, tested at a current density of 20 mA g⁻¹. By an electrochemical self-doping of an amorphous TiO₂ nanotube array and N₂ annealing, Kim et al. developed a black-colored TiO₂ nanotube array that displayed high capacitance, satisfactory electrocatalytic performance, good stability, and an excellent material for supercapacitors and oxide anodes [134].

Antibacterial Activity

Bacteria's resistance to antibiotics due to its misuse has become a global crisis and nanoparticles (NPs) are being considered as a potential drug alternative to overcome this bacterial multidrug resistance. Nanoparticles can override bacterial resistance by coming into direct contact with the bacterial cell wall, without needing to penetrate the cell itself. Nanomaterials have shown substantial antimicrobial activity against both Gram-positive and Gram-negative bacteria, mycobacteria, and fungi [135]. The physical structure of the nanoparticle itself may have inherent antibacterial characteristics due to its abrasiveness that causes damage to the bacterial membrane, as seen in graphene oxide nanoparticles. It has been observed that the high surface-to-volume ratio of the

nanoparticles can increase antimicrobial activity as it allows an improved interaction of the nanomaterials with the surrounding environment. Particle size, particle shape, chemistry, and zeta potential are among the most relevant variables affecting antibacterial activity [135]. Guided release of antibacterial metal ions from the surface of nanoparticles has also been suggested.

The antimicrobial activity of heavy metals such as silver (Ag), copper (Cu), gold (Au), titanium (Ti), and zinc (Zn) has been known to humans for centuries. The Rasashastra of the Ayurvedic system of medicine deals with drugs of mineral origin [136]. Evidence of the use of the medicine of mineral origin in China's Song dynasty has also been found [137]. Among various nanoparticles, substantial antimicrobial activities have been exhibited by metallic oxides. Silver oxide (Ag₂O), titanium dioxide (TiO₂), copper oxide (CuO), zinc oxide (ZnO), calcium oxide (CaO), magnesium oxide (MgO), silicon (Si), gold (Au), etc. are significantly active against a wide array of microorganisms [138]. Many factors can affect the toxicity of the NPs, including their shape, size, surface charge, composition, and stability. The US Food and Drug Administration (FDA) has approved the use of several types of nanoparticles including silver and titanium derivatives for products such as antibacterial skin lotions and sunscreens which are already in commercial use.

It has been observed that reactive oxygen species act in concert to attack polyunsaturated phospholipids in bacteria and also catalyze DNA damage by generating H₂O₂ which result in the death of bacterial cell [139]. ZnO NPs have shown substantial antimicrobial activity against common food pathogens such as *Campylobacter jejuni*, *E. coli* O157:H7, *Salmonella* spp., *Listeria monocytogenes*, and *S. aureus*, indicating its usefulness as a food preservative. They can block the growth of both Gram-positive and Gram-negative bacteria. Gram-positive bacteria including *S. aureus*, *Streptococcus pyogenes* and *Enterococcus faecalis* have shown 95% growth inhibition in the presence of ZnO nanoparticles [140]. Silver nanoparticles have also shown synergistic activity with common antibiotics that are used today including ampicillin, erythromycin,

clindamycin, penicillin G, and vancomycin against *E. coli* and *S. aureus* [141]. Ag NPs are particularly used as a coating material for textiles, medical devices, refrigerators, and food containers for their substantial antibacterial properties. The antimicrobial activity of copper NPs has been observed against a wide array of bacteria and yeast. They are active against methicillin-resistant *S. aureus* (MRSA) and *Bacillus subtilis*, Gram-negative organisms such as *S. choleraesuis* and *P. aeruginosa*, and yeast species such as *Candida albicans* [135].

Drug Delivery

It has been observed that TiO₂ with a high specific surface area can be advantageous in drug delivery carrier applications. Through surface energy and pore size control, Johan et al. controlled the kinetics of drug delivery from mesoporous titania thin films [142]. By the use of different structural guiding templates and expansive agents, different pore sizes ranging from 3.4 nm to 7.2 nm were achieved. In addition, the surface energy of the pore wall could be altered by attaching dimethyl silane to the pore wall. The results inferred that the pore size and surface energy had significant effects on the adsorption and release kinetics of alendronate [142].

To cure breast cancer by effectively delivering doxorubicin (DOX) to the cancer cells, Biki et al. designed silica-supported mesoporous titania nanoparticles (MTN) coated with hyaluronic acid [143]. To overcome the drug resistance of tumors, Guo et al. deposited (onto the surface of MTN) hyaluronic acid and cyclic pentapeptide (ADH-1), which target CD44-overexpressing tumor cells and selectively inhibit the function of N-cadherin, respectively [144]. Nakayama et al. demonstrated that H₂O₂-treated TiO₂ can enhance the production of reactive oxygen species (ROS) in response to X-ray irradiation [145]. Dai et al. designed and synthesized a novel nano-drug delivery system for the treatment of lung cancer with a synergistic effect [146]. They loaded DOX onto H₂O₂-treated TiO₂ nanosheets and in this method, chemotherapy and radiotherapy were combined effectively for the synergistic therapy of cancers.

Textiles

Nanoparticles are being used in apparel and filters because of their multi-functionality including water repellency, vapor transmission, thermal storage, antifouling, deodorizing, and antibacterial properties. N-doped TiO₂-supported fibers are particularly useful because they can effectively provide these functionalities due to oxidative decomposition properties under visible-light illumination [147]. It has been demonstrated that inactivation rates of the influenza virus are more than 99.9% under UV light irradiation and more than 98.3% under fluorescent light irradiation.

Various studies have demonstrated that fiber properties are improved by nano-decorating textiles with active particles, which may include gaining water repellency [148], increased mechanical strength [149], wrinkle resistance, antistatic, color change [150] or UV protection [151]. Among all nanoparticles, TiO₂ turned out to be the most effective and cheap alternative for textile coatings [152]. Recently, many articles have focused on the functionalization of textiles with TiO₂ NPs and their self-cleaning properties [153], [154]. Various photocatalytic fibers based on cotton [155], polyester [156], wool [157], etc. were designed and, despite the changes that might have occurred during the functionalization process, these materials remain harmless to the skin cells. For example, it has been demonstrated that nano TiO₂-coated fabrics exhibit great antibacterial efficiency against *Escherichia coli* and *Staphylococcus aureus* and antifungal activity against *Candida albicans*, along with a significant self-cleaning capacity and no cytotoxic effects on human skin fibroblasts [158].

Veronovski et al. reported that self-cleaning fabrics can be obtained by applying an active photocatalytic layer containing the oxide of a transition metal [159]. This coating reacts with organic compounds or pollutants deposited on the fabric and decomposes them under sunlight into simple inorganic compounds such as CO₂ and H₂O which are subsequently removed by heat, wind or rain. Fiber degradation is another issue related to the photoactivity of TiO₂. Veronovski and her team developed a titanium-silica composite shell that can be applied to avoid the negative impact on fibers. However, any applied pre-treatment only modifies the outer superficial layers of

the fabric without affecting its inherent properties. A real-life application of these so-called “smart” textiles was introduced by US Army in collaboration with the Massachusetts Institute of Technology. They have invented a waterproof, lightweight, and breathable uniform that can kill bacteria. Furthermore, for protection against chemical or biological weapons during wars, scientists have attempted to develop "nanopores" in soldiers' uniforms that can close automatically when chemical or biological agents are detected.

Anti-fogging Effect

The anti-fogging effect is another useful aspect of TiO₂ nanoparticles based on their hydrophilic nature. Fogging occurs when steam cools down on the surfaces of mirrors and glasses to form water droplets which can be very disturbing at times. On an effective hydrophilic surface, a uniform thin film of water is formed which prevents the accumulation of water droplets, hence fogging.

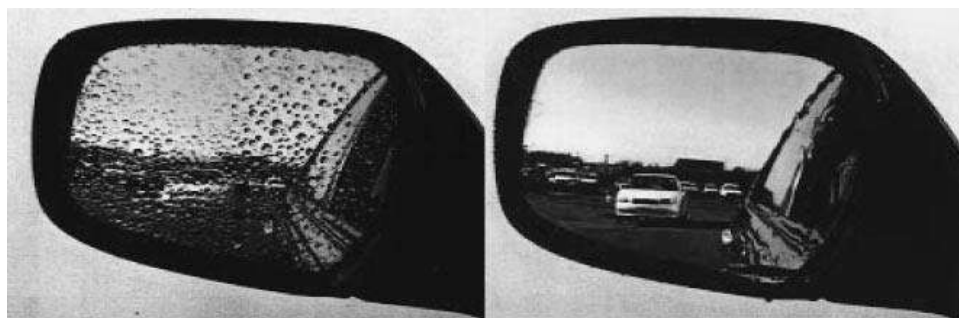


Figure 2.12: Anti-fogging effect of automobile side-view mirror: conventional mirror (left) and TiO₂-coated hydrophilic mirror (right) [23].

The surface can retain this state for up to one week [23]. Therefore, this property can be applied to various glass products such as eyeglasses, mirrors, etc. Many Japanese car manufacturers have started to equip their cars with mirrors having antifogging properties as shown in **Figure 2.12**.

CHAPTER 3: EXPERIMENTAL METHODOLOGY

3.1 Materials Synthesis

Synthesis of undoped and Fe-doped TiO₂

Undoped and Fe-doped TiO₂ were prepared by sol-gel synthesis. The raw materials used in this research are the following:

- a. Titanium (IV) butoxide/ tetrabutyl titanate (TBT) (from Sigma-Aldrich as a precursor).
- b. Absolute ethanol (from Hayman Ltd. England as solvent).
- c. Acetic acid glacial (UN2789) (from Ghtech China as an inhibitor. Acetic acid further catalyzes crystallization).
- d. Iron (III) nitrate nonahydrate/ ferric nitrate (Fe(NO₃)₃·9H₂O) (from Sigma-Aldrich as doping source).
- e. Iso-propanol (from Changshu Yangyuan Chemical, China for making coating suspension).
- f. Distilled water.

All the chemicals were AR (analytical reagent) grade. Ping Yu et al. [60], Ramalingam et al. [62], Li et al. [148], and Sood et al. [149] also used TBT as a precursor and Fe(NO₃)₃·9H₂O as an iron doping source to synthesize Fe-doped TiO₂.

Step 1: Preparation of undoped TiO₂

Firstly, solution-A was prepared by adding and mixing TBT, acetic acid, and absolute ethanol.

Secondly, solution-B was prepared by adding and mixing acetic acid, distilled water, and absolute ethanol. Solution-B was added dropwise into solution-A with vigorous magnetic agitation. The obtained mixture was stirred for 4 h, followed by aging for more than 24 h, which resulted in gel formation. This gel was dried at 100°C in the oven and reduced into powder using mortar and pestle. The obtained powder is then annealed at 500°C at a rate of 3°C/min in a programmable furnace for 3 h. The final powder obtained was undoped TiO₂.

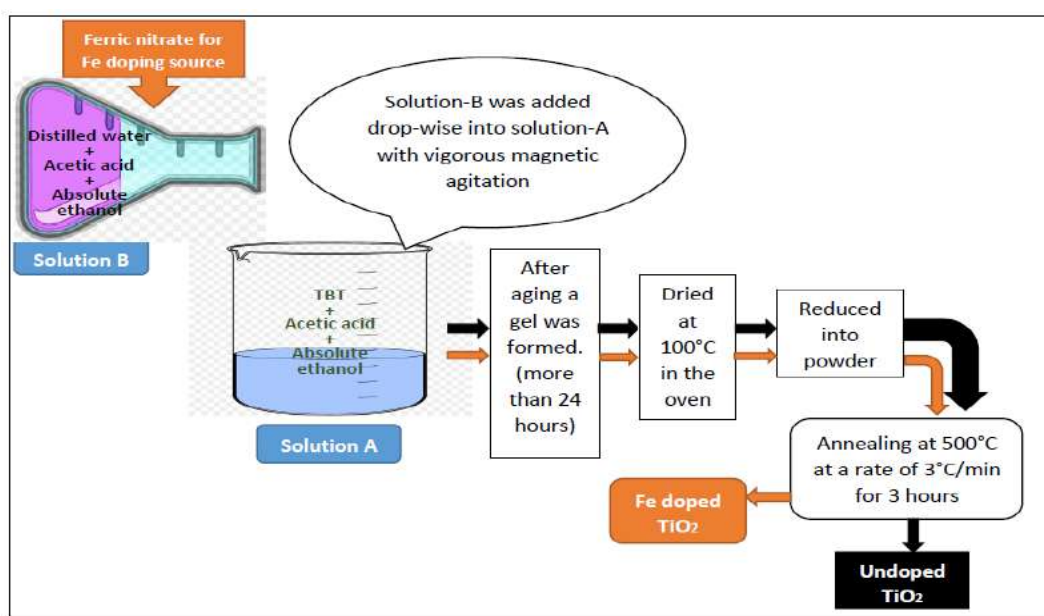


Figure 3.1: Schematic process for the synthesis of undoped and Fe-doped TiO₂.

Step 2: Preparation of Fe-doped TiO₂

The Fe-doped TiO₂ (Ti_{1-x}Fe_xO₂, x = 0.01 to 0.04) was prepared using the same procedure, while dopant source ferric nitrate was added in solution-B.

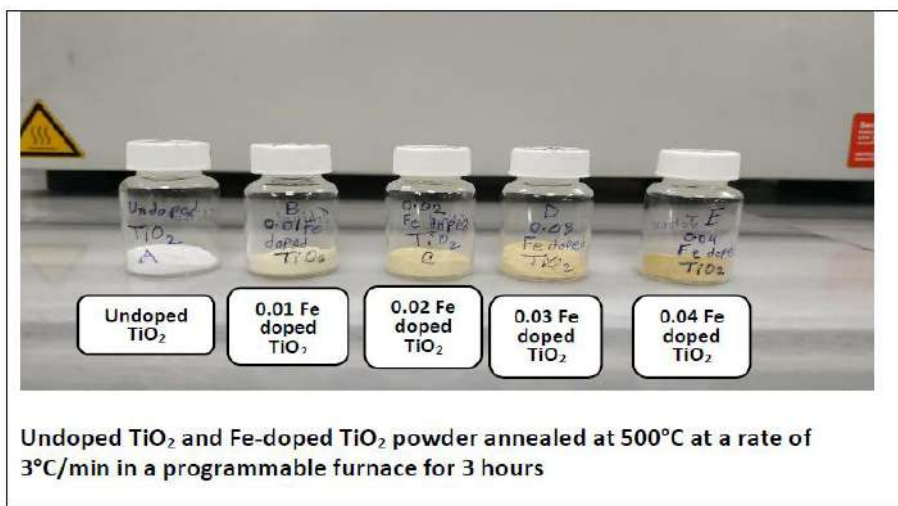
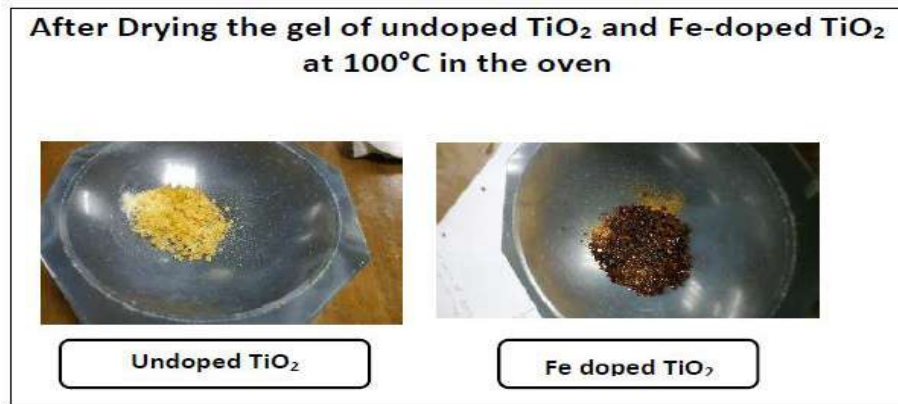
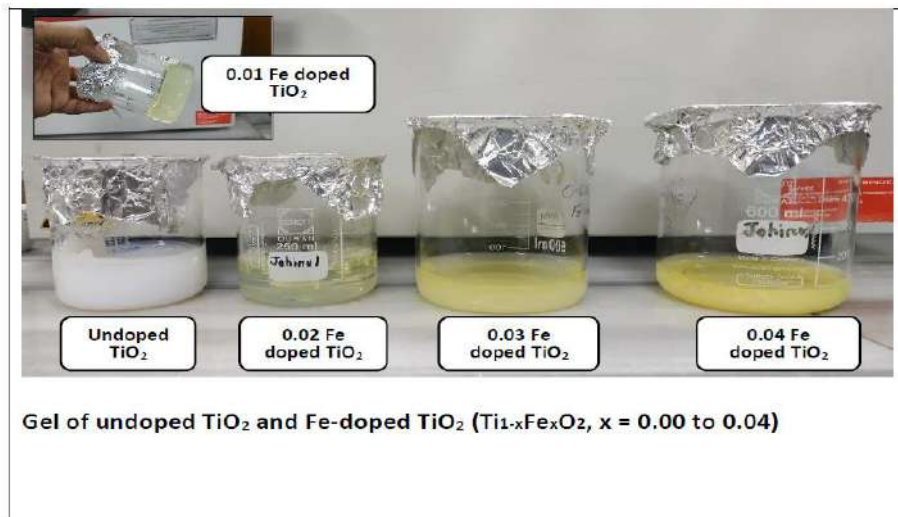


Figure 3.2: Physical appearances of undoped and Fe-doped TiO₂ at different steps of synthesis (i) After gel formation; (ii) After drying; (iii) After grinding and annealing.

Step 3: Preparation of photocatalyst-coated glass surfaces

Photocatalyst-coated glass surface for every sample was prepared by a dip coating method. At first coating suspensions of each photocatalyst powder and iso-propanol were prepared for making photocatalyst-coated glass surfaces. The ratio of each photocatalyst powder and iso-propanol was 1:10. The suspension-coated glass surfaces were then dried in an oven at 83°C for 1 h. Photocatalyst-coated glass surfaces for every sample were prepared in similar way.

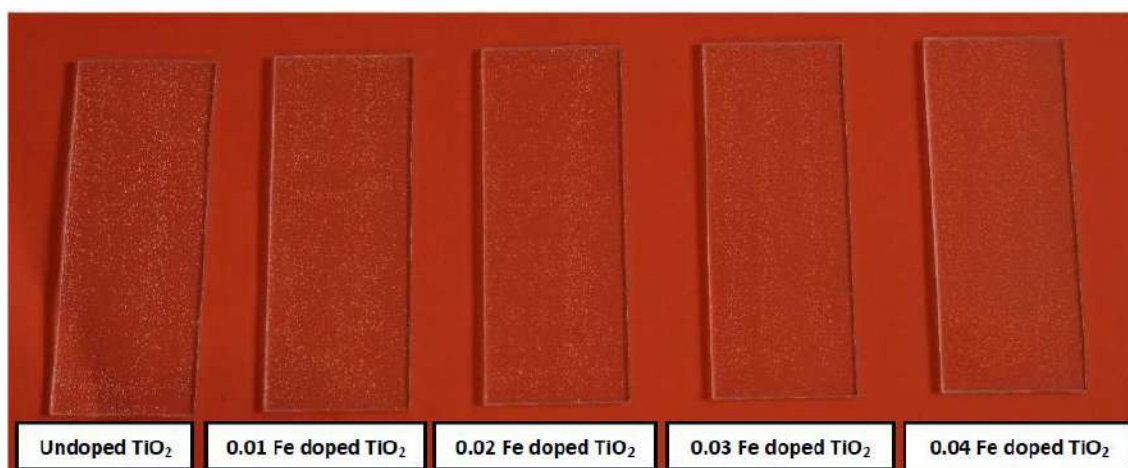


Figure 3.3: Photocatalyst-coated glass surfaces.

3.2 Characterization of the Undoped and Fe-doped TiO₂ Samples

The structural, optical, and morphological analysis of undoped and Fe-doped TiO₂ samples were performed using X-Ray Diffraction, UV-Vis-NIR diffuse reflectance spectroscopy, and Field-emission Scanning Electron Microscopy, respectively. Moreover, the photocatalytic activity and self-cleaning performance of all samples were tested by photocatalytic dye degradation experiment and hydrophilic conversion test.

3.2.1 FESEM Analysis

The surface morphology of the synthesized nanoparticles was observed using JSM 7600F, JEOL (Japan) Field Emission Scanning Electron Microscope. The images were taken using 5 kV at magnifications of x100,000. Particle size analysis for each sample was carried out from these FESEM images by using ImageJ software.

3.2.2 X-Ray Diffraction Analysis

To obtain the crystalline phases present in the synthesized samples as well as crystallite size, lattice parameters, and other crystallographic information, X-Ray Diffraction (XRD) technique was carried out. The XRD analysis of the samples was performed by X-Ray Diffractometer (PANalytical, Netherlands) with radiation source Cu K α (wavelength 1.54Å) at 2 θ range 10-80°. The powder samples were placed on a non-diffracting sample holder positioned in the Bragg-Brentano diffractometer setup. Rietveld refinement was performed using software (HighScore Plus 4.1) before calculating the crystallite sizes, FWHM, and lattice parameters of the samples.

3.2.3 UV-Visible Spectroscopy Analysis

To determine the optical absorption edge of the samples, Diffused Reflectance Spectra of all samples were collected using LAMBDA 1050, PerkinElmer (USA) UV-Vis-NIR Spectrophotometer from wavelengths 200-800 nm at 25°C. From the diffused reflectance spectra, the optical absorbance of the samples was measured.

3.2.4 Photocatalytic Dye Degradation Experiment

Photocatalytic degradation of the aqueous solution of Methylene blue (MB) was investigated under UV-A light and LED light (as visible light irradiation) separately. Both UV-A and LED lights had a capacity of 100W. *Azami et al.* also selected LED light as a visible light source for the photocatalytic dye degradation experiment [160]. The photocatalytic nanoparticles of 0.15 g of each sample were dispersed in a 500 ml MB solution (20 mg/l) in an ultrasound generator for 10 min. After stirring the suspension for 30 min in the dark to achieve adsorption equilibrium, the photocatalytic

activity of the catalyst was tested. The Undoped TiO_2 sample was observed under both UV-A radiation and visible light illumination separately. Fe-doped TiO_2 samples of different concentrations were observed under visible light illumination. The time duration of observation for undoped and Fe-doped samples was 6 h. The reactive solutions will be withdrawn at intervals. The residual concentration of MB solutions was measured with a UV-Vis spectrophotometer. The high-intensity characteristic absorbance band at 663 nm indicated the initial concentration of MB.

For keeping the samples under UV-A radiation and visible light illumination separately, an arrangement of the box was prepared (**Figure 3.4**) to test the photocatalytic activity of the samples. The samples were kept inside the box in such a way that no other light radiation from outside can enter the box. As a result, the samples were observed under our desired light radiation only.

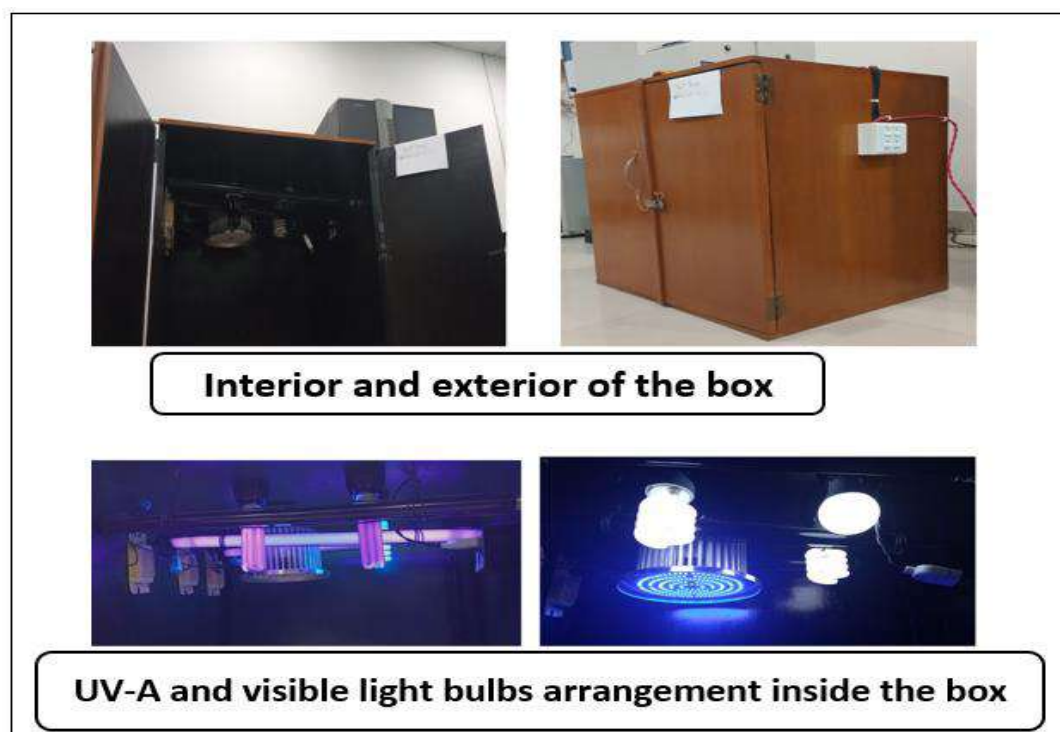


Figure 3.4: Prepared box with the arrangement of UV-A and visible light bulbs for checking the photocatalytic activity of the samples.

3.2.5 Hydrophilic Conversion Test

The hydrophilicity of a surface can be measured by the contact angle of a water droplet on the surface. Contact angle (θ) is defined as the angle between a liquid and a solid surface at the interface of a solid, a liquid, and a vapor. A surface with less than a contact angle of 90° is called hydrophilic. A hydrophobic surface is one having a contact angle of more than 90° . A surface having a contact angle of less than 10° is known as superhydrophilic and more than 150° as superhydrophobic. The wettability of a surface can be determined by the contact angle.

The hydrophilicity of each coated surface was measured by the contact angle of a water droplet on each surface. Before putting the water droplet on the coated surface, the undoped TiO_2 -coated glass surface was kept under UV-A and visible light illumination separately. On the other hand, Fe-doped TiO_2 -coated glass surfaces with different Fe concentrations were kept under only visible light illumination. Time durations for both undoped and Fe-doped TiO_2 -coated surfaces were 2 h. To determine the contact angle of a water droplet on each photocatalyst-coated glass surface, a digital camera containing a macro lens was used. Photos of tiny little droplets on each photocatalyst-coated glass surface were taken by this camera very carefully so that the plane of the coated glass surface and the plane of the camera lens remains at a 90° angle. Using these HD photos, the contact angles of the water droplet on each photocatalyst-coated glass surface were measured.

CHAPTER 4: RESULTS AND DISCUSSION

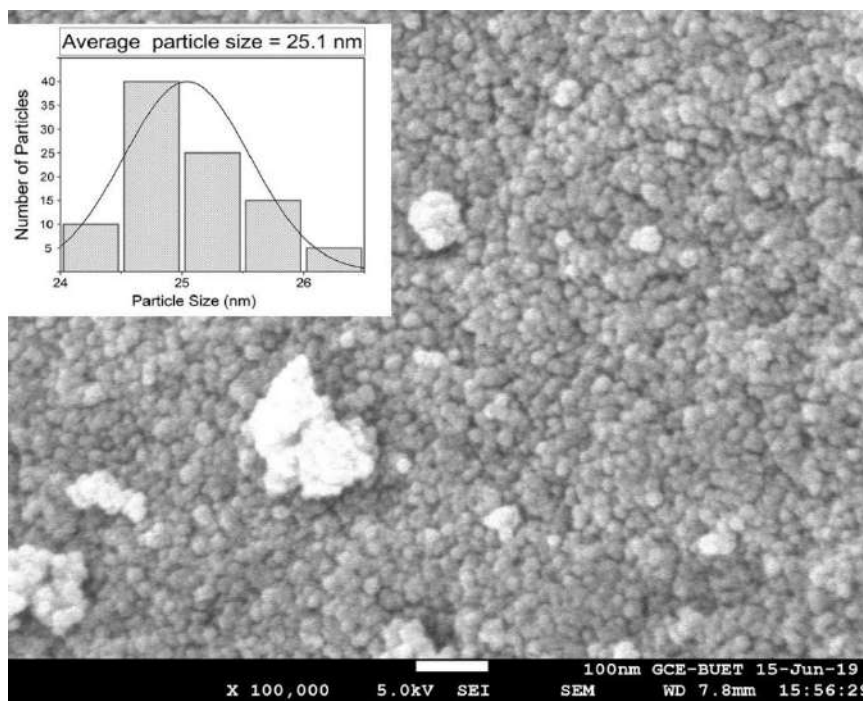
4.1 Morphology Analysis by FE-SEM

The morphology and particle size of the samples were studied by Field Emission Scanning Electron Microscope (FESEM) analysis. SEM images of undoped and Fe-doped TiO₂ samples are provided in **Figure 4.1**. According to FESEM analysis, both undoped and Fe-doped particles are spherical. Particle sizes were measured by using ImageJ software from the SEM images of each sample. The average particle sizes of each sample are listed in **Table 4.1**. The particle size of undoped TiO₂ was found to be almost uniform. But in the case of Fe-doped TiO₂ samples, particle size varied randomly which is due to the effect of Fe doping on TiO₂ nanoparticles. It was observed that average particle size reduces with Fe doping. The ionic radius of Ti⁴⁺ is about 0.68 Å and Fe³⁺ is about 0.64 Å [69], [161]. Reduction of particle sizes with Fe doping indicates the probability of some Ti⁴⁺ ions being replaced by Fe³⁺ ions within the crystal framework of TiO₂ [162], [163].

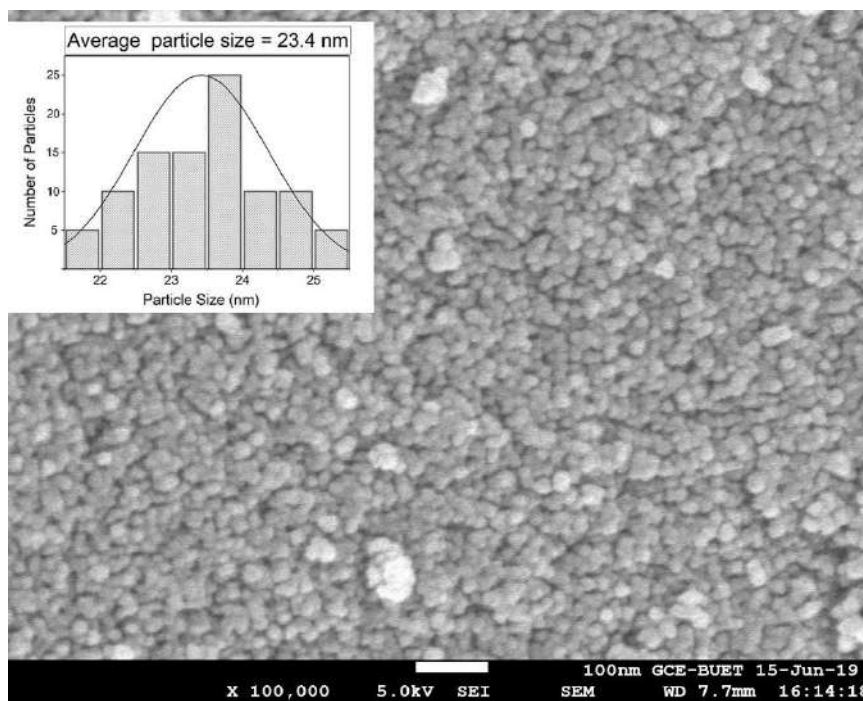
Table 4.1: Average particle sizes of pure and Fe-doped TiO₂ samples

	Average particle size (nm)
Undoped TiO ₂	25.05
Fe _{0.01} -doped TiO ₂	23.42
Fe _{0.02} -doped TiO ₂	22.39
Fe _{0.03} -doped TiO ₂	21.3
Fe _{0.04} -doped TiO ₂	20.27

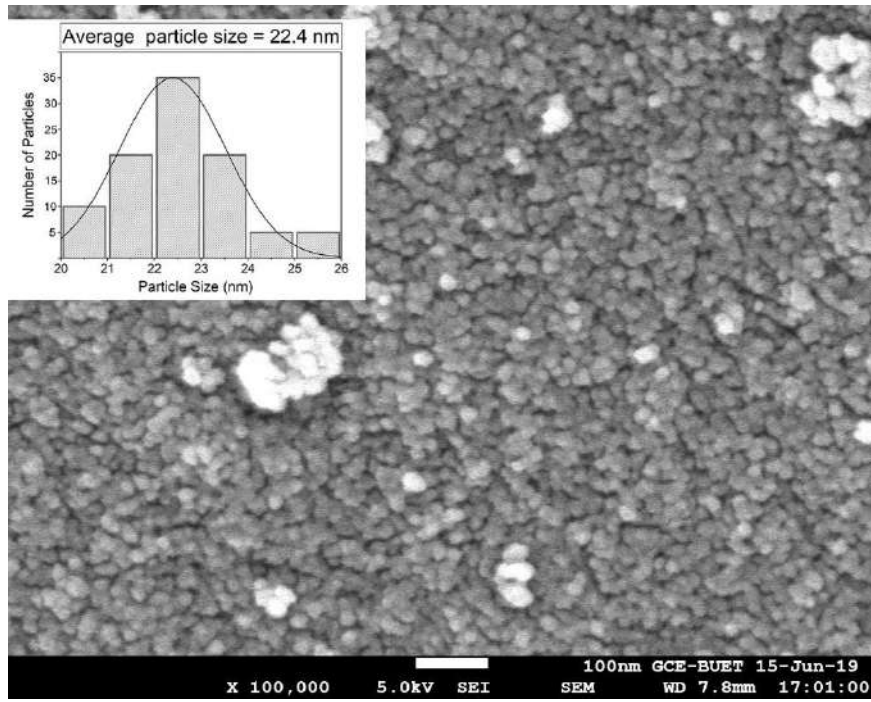
A. Undoped TiO₂



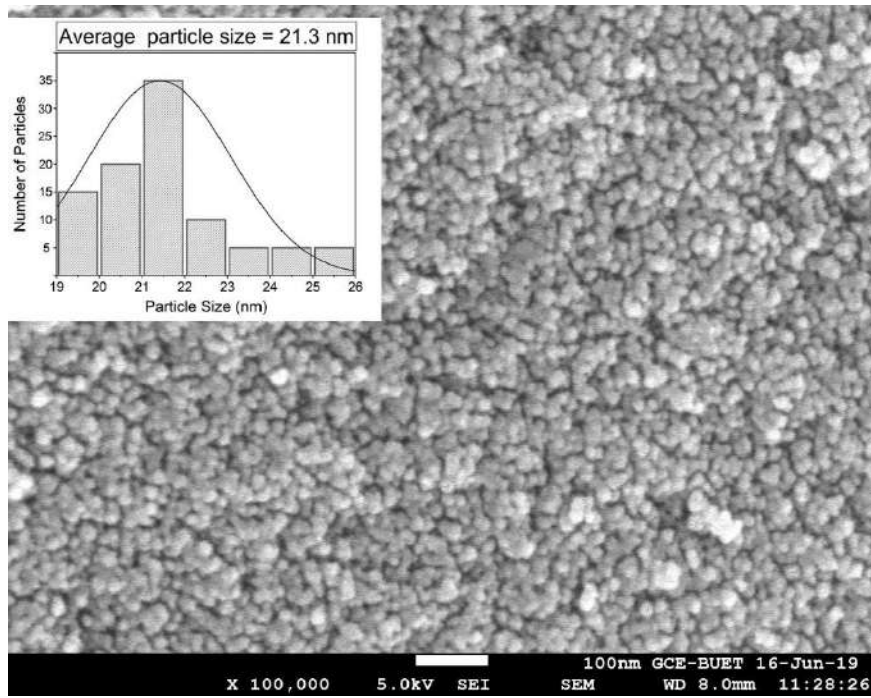
B. Fe_{0.01} doped TiO₂



C. Fe_{0.02} doped TiO₂



D. Fe_{0.03} doped TiO₂



E. Fe_{0.04} doped TiO₂

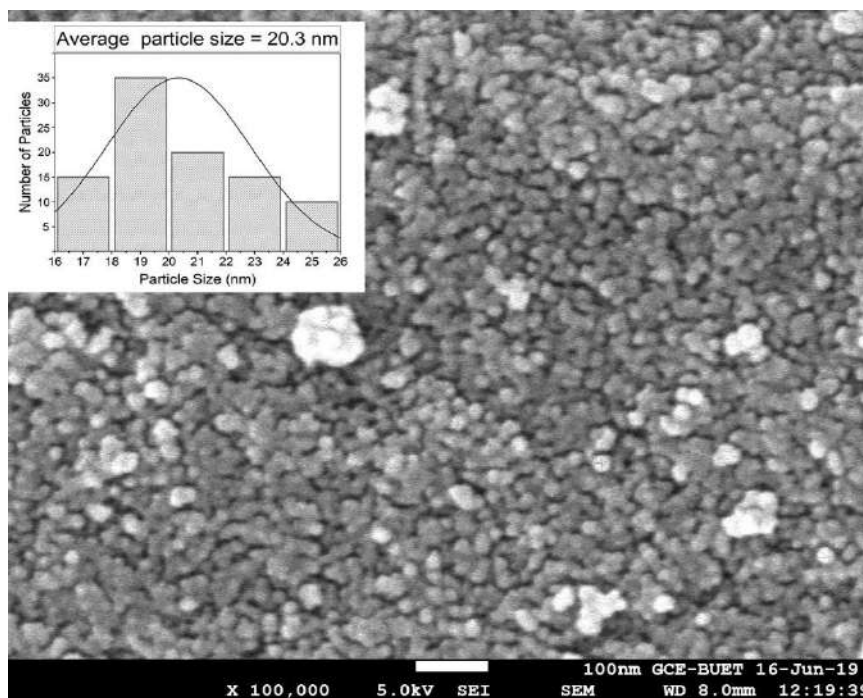


Figure 4.1: FE-SEM images of the samples at magnification x 100,000. (A) Undoped TiO₂ (B) Fe_{0.01} doped TiO₂ (C) Fe_{0.02} doped TiO₂ (D) Fe_{0.03} doped TiO₂ (E) Fe_{0.04} doped TiO₂.

4.2 Structural Analysis by X-Ray Diffraction

Figure 4.2 shows the XRD patterns of undoped and Fe-doped TiO₂ samples. The Bragg peaks of the XRD line profiles are completely matched with the anatase phase of TiO₂ (ICSD database code: 9853, Space group: I 41/a m d (141)). No Bragg peaks of any second phase were observed within the XRD detection limit, indicating that no other phase is present in both undoped and Fe-doped TiO₂ samples. The Bragg angles and the corresponding planes are listed in **Table 4.2** and **Figure 4.2**, confirming the peaks of the pure anatase phase of TiO₂ for all samples. Generally, 500°C annealing temperature is used to obtain anatase structure as anatase to rutile phase transition occurs in a wide temperature range of 600°C –1100°C [57], [161], [164]. Yu et al. in their research on the preparation of N, Fe co-doped TiO₂ Photocatalyst by sol-gel method also found pure

anatase structure at 500°C annealing temperature [72]. In this work, a 500°C annealing temperature was also used to obtain the pure anatase phase.

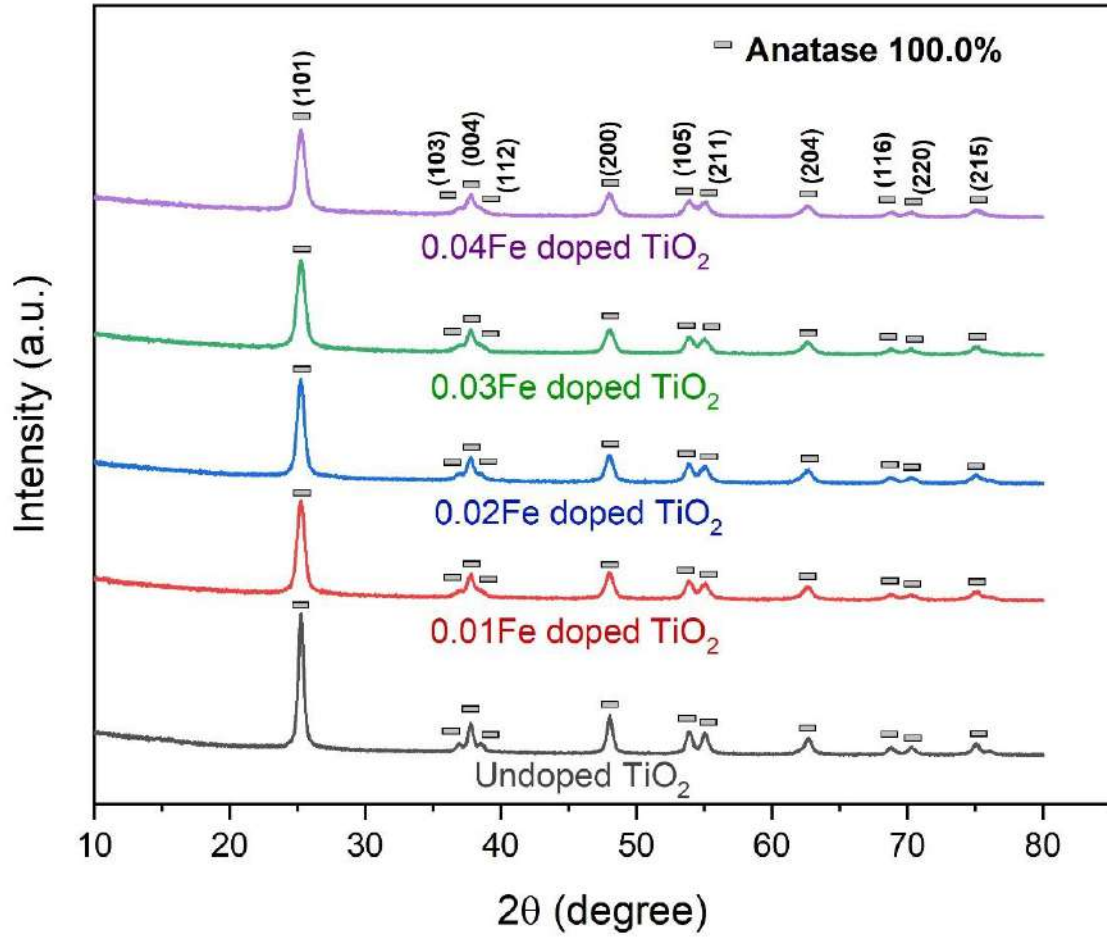


Figure 4.2: XRD patterns of undoped and Fe-doped TiO₂ samples. All Bragg peaks are indexed according to their corresponding crystallographic planes.

Table 4.2: The Bragg angles and the corresponding crystallographic planes of obtained sample confirm the anatase phase

Sl.	2 θ	h	k	l
1	25.30	1	0	1
2	36.93	1	0	3
3	37.79	0	0	4
4	38.54	1	1	2
5	48.02	2	0	0
6	51.95	2	0	2
7	53.91	1	0	5
8	55.05	2	1	1
9	62.11	2	1	3
10	62.70	2	0	4
11	68.79	1	1	6
12	70.30	2	2	0
13	74.12	1	0	7
14	75.08	2	1	5
15	76.04	3	0	1
16	78.71	2	0	6

The information on lattice parameters and the unit cell volumes of the samples were obtained from the Rietveld analysis of the XRD patterns (**Table 4.3**). As all the samples show only anatase structure, their lattice structure is tetragonal with a slight change in crystal size. The radius of Fe³⁺ (0.064 nm) is smaller than that of Ti⁴⁺ (0.068 nm) [69], [161]. While entering into the TiO₂ lattice, Fe³⁺ doesn't break the crystal structure but inhibits the growth of the particle size. Therefore, this may be the reason for the broadening of the peak width and decrease in particle size of Fe-doped TiO₂ with increasing the concentration of Fe (**Table 4.3**) [77], [162]. Smaller particle size increases the surface area, which favors better photocatalytic activity [164]. Moradi et al. [165], Sood et al. [163], and Li et al. [166] also observed a decrease in particle size with Fe-doping in their experiment. The average crystallite sizes of all samples in **Table 4.3** were calculated by using Debye–Scherrer Formula.

$$\text{Debye-Scherrer Formula: } D = \frac{0.94\lambda}{\beta \cos\theta}$$

Where,

D= Average crystallite size or particle size

β = FWHM or width of the diffraction peaks at half height (rad) or line broadening in radians

θ =Bragg angle

λ = X-Ray wavelength 0.15406 nm

Table 4.3: Comparison of average crystallite size obtained from XRD and average particle size from SEM

Sample Name	Lattice Parameters	Cell Vol. (x 10 ⁶ pm ³)	FWHM	Average crystallite size from XRD	Average particle size from SEM
Undoped TiO₂	a = 3.784154 Å b = 3.784154 Å c = 9.508555 Å $\alpha = \beta = \gamma = 90^\circ$	136.16	0.51	16.67	25.05
Fe_{0.01} doped TiO₂	a = 3.784752 Å b = 3.784752 Å c = 9.504419 Å $\alpha = \beta = \gamma = 90^\circ$	136.14	0.65	13.08	23.42
Fe_{0.02} doped TiO₂	a = 3.784569 Å b = 3.784569 Å c = 9.501848 Å $\alpha = \beta = \gamma = 90^\circ$	136.09	0.67	12.69	22.39
Fe_{0.03} doped TiO₂	a = 3.784532 Å b = 3.784532 Å c = 9.499923 Å $\alpha = \beta = \gamma = 90^\circ$	136.06	0.71	11.97	21.3
Fe_{0.04} doped TiO₂	a = 3.783631 Å b = 3.783631 Å c = 9.503588 Å $\alpha = \beta = \gamma = 90^\circ$	136.05	0.75	11.31	20.27

4.3 Optical Analysis by UV-Vis Spectroscopy

The photocatalytic activity of TiO₂ is related to the range of its spectral response. **Figure 4.3** shows UV–Vis absorption spectra of undoped and Fe-doped TiO₂ samples. Planck's equation, Tauc Plots, and Kubelka-Munk function are used to calculate the band gap and optical absorption edge of all samples. Kubelka-Munk function is based on a standard Tauc plot and generally uses the intercept of the extrapolated straight line with the energy/wavelength axis at $(\alpha hc/\gamma)^n = 0$ which indicates that there is no absorption fall beyond the slope point. However, for the samples where the absorption tail is not parallel to the energy/wavelength axis, the extrapolated energy value of the intersection of two linear portions of the absorption curve could be more useful to estimate the optical band gap.

Planck's equation: $E = \frac{hc}{\lambda}$

The equation used for obtaining Tauc Plot: $(\alpha hc/\gamma)^n = A(h\nu - E)$

Where,

E = Band gap energy in eV,

h = Planks constant,

C = Velocity of light,

λ = Wave length,

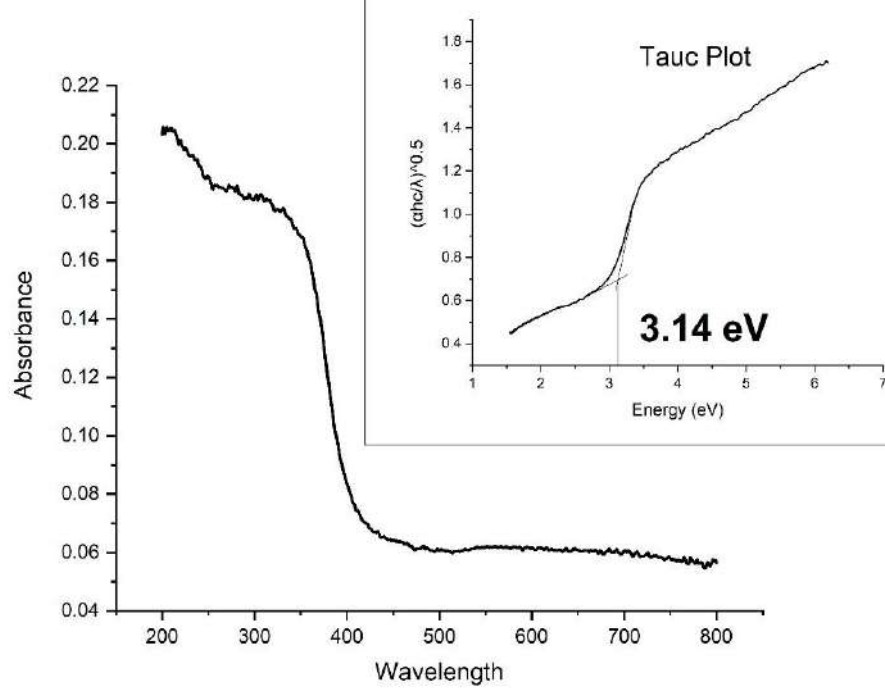
ν = Photon's frequency,

α = Absorption coefficient,

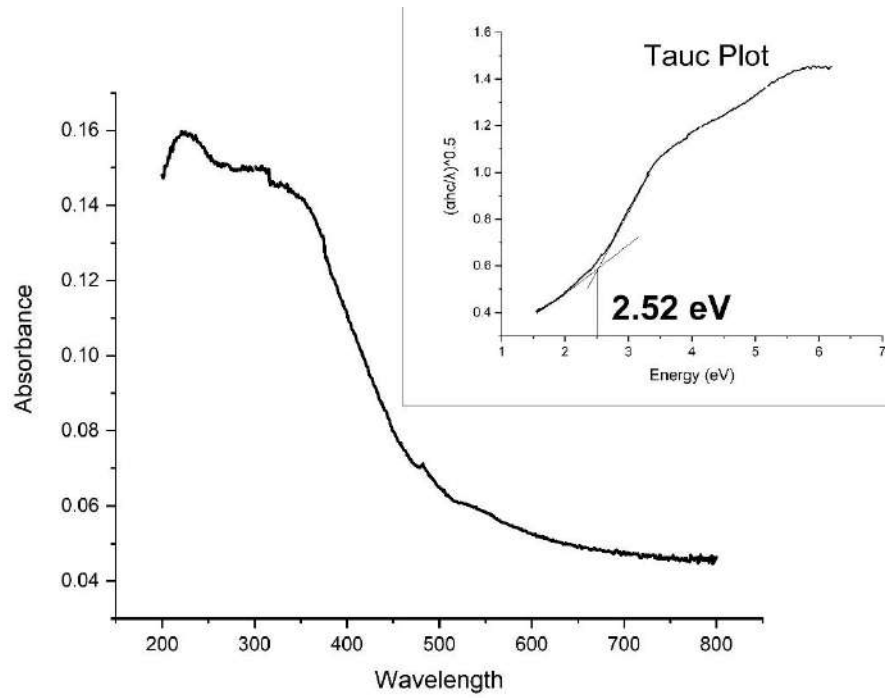
A = Proportionality constant, and

n = 0.5 for indirect band-gap

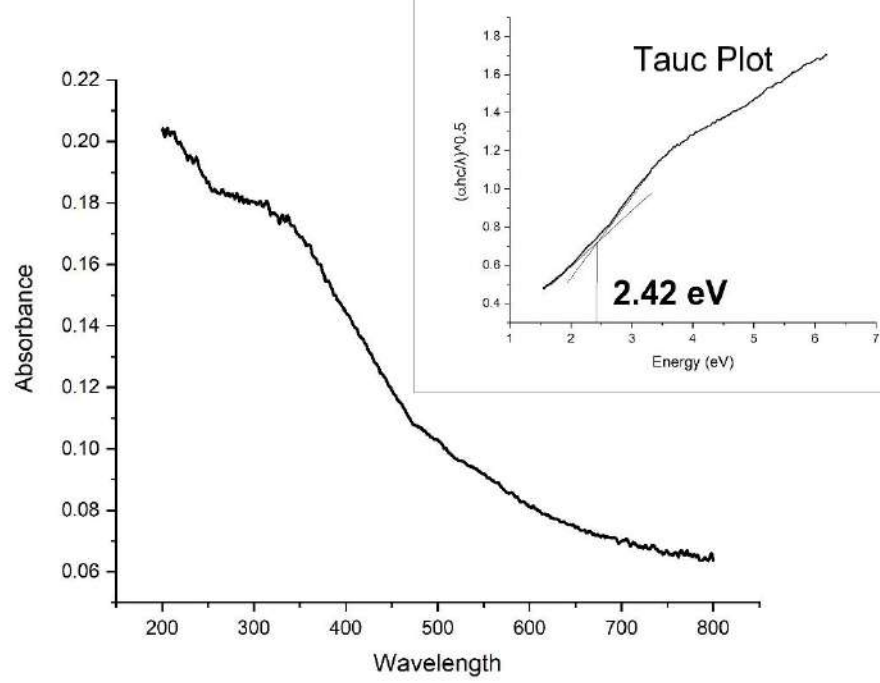
A. Undoped TiO₂: Band gap 3.14 eV



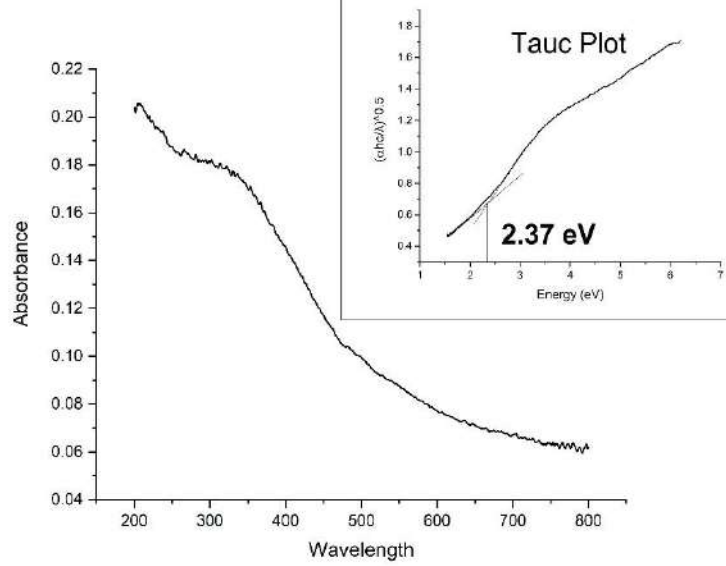
B. Fe_{0.01}-doped TiO₂: Band gap 2.52 eV



C. Fe_{0.02}-doped TiO₂: Band gap 2.42 eV



D. Fe_{0.03}-doped TiO₂: Band gap 2.37 eV



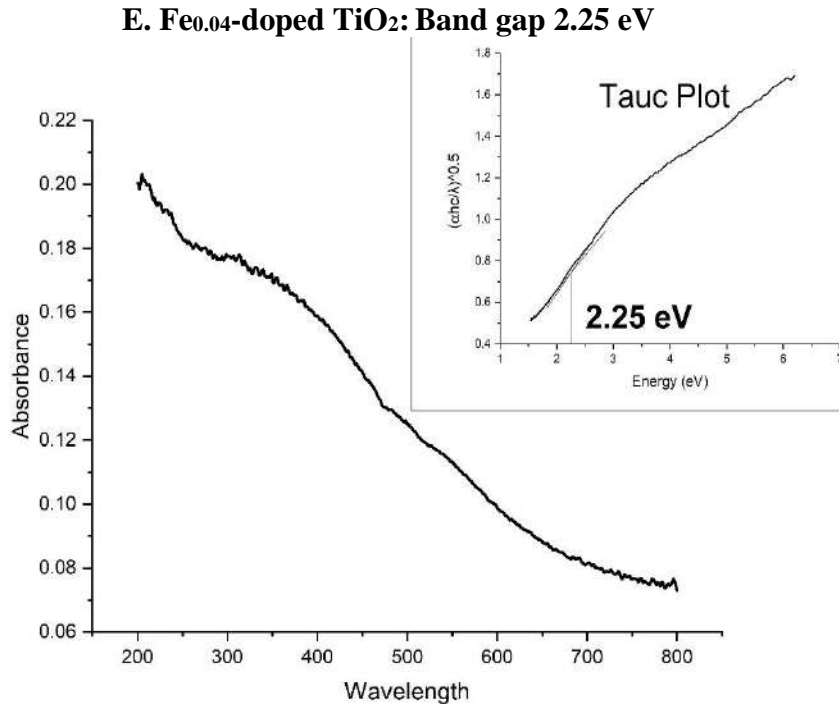


Figure 4.3: UV-Vis absorbance spectra of the samples. (A) Undoped TiO₂ (B) Fe_{0.01} doped TiO₂ (C) Fe_{0.02} doped TiO₂ (D) Fe_{0.03} doped TiO₂ (E) Fe_{0.04} doped TiO₂.

The pure TiO₂ sample almost had no response to visible light and the absorbing edge was at approximately 395 nm. The optical absorbing edges of Fe_{0.01}, Fe_{0.02}, Fe_{0.03}, and Fe_{0.04} doped TiO₂ were extended to approximately 492 nm, 512 nm, 523 nm, and 550 nm. The shift in the absorption band edges of the Fe-doped TiO₂ samples indicates that the optical band gap decreases with Fe doping. The band gap of pure TiO₂ was about 3.14 eV. On the other hand band gaps of Fe_{0.01}, Fe_{0.02}, Fe_{0.03}, and Fe_{0.04} doped TiO₂ were reduced to approximately 2.52 eV, 2.42 eV, 2.37 eV, and 2.25 eV. It may be attributed to the Fe dopant that entered into the TiO₂ lattice and narrowed the band gap to extend the visible response [15], [163], [164], [166]. A new energy level is created by doped Fe ions below the conduction band of TiO₂ by which a red shift in the absorption band edge occurs [69], [167].

4.4 Photocatalytic Activity Analysis by Methylene Blue Degradation

The photocatalytic activity of a photocatalyst is related to the range of its spectral response. **Figure 4.4** and **Table 4.4** show the effect of the photocatalytic reaction of both undoped and Fe-doped TiO₂. **Figure 4.4(A)** represents the photocatalytic degradation of MB solution indicated in the Y-axis as C/C_0 . Where, C is the concentration of MB after a specific time and C_0 is the initial concentration of MB ($C_0 = 20$ ppm MB solution). **Figure 4.4(B)** indicates the percentage of MB degradation with respect to time. Photocatalytic degradation of MB solution containing undoped TiO₂ was carried out under UV and visible light illumination separately. In the case of undoped TiO₂ under UV radiation, 75% MB was degraded. As undoped TiO₂ is not particularly active under visible light, only 7% MB was degraded during visible light illumination.

In the case of Fe-doped TiO₂ under visible light illumination, the degradation percentage of MB increased. MB degradation was increased with the increase of Fe doping at a certain level. The MB degradation percentages of Fe_{0.01}, Fe_{0.02}, Fe_{0.03} and Fe_{0.04} doped TiO₂ in visible range were 19%, 30%, 60%, 26%, respectively. Among Fe-doped TiO₂ under visible light illumination, Fe_{0.03}-doped TiO₂ was able to provide an enhanced photocatalytic reaction. Further increasing of Fe doping lowered the photocatalytic reaction.

The conduction band minimum of TiO₂ consists of Ti d states. A lower energy level was introduced by Fe doping in the TiO₂ lattice. Due to the narrowing of the band gap of Fe-doped TiO₂, successfully yielded a redshift of the light absorption [69], [166], [167]. The holes and electrons are generated under visible light irradiation which are then trapped by the Fe ions [168]. Subsequently, the Fe³⁺ ions appear again by generating hydroxyl radicals ($\cdot\text{OH}$) and superoxide (O_2^-) groups. Thus Fe doping enabled the photocatalytic reaction of Fe-doped TiO₂ under visible light illumination [15], [69], [163]. Fe³⁺ can trap both electrons and holes up to an optimum amount of doping. However, recombination centers can appear if doping is further increased. This can lead to the reduction of the photo-generated charge carriers resulting in less photocatalytic

reaction [15], [69], [163], [168]–[170]. That’s why $\text{Fe}_{0.04}$ -doped TiO_2 yielded lesser MB degradation than $\text{Fe}_{0.03}$ -doped TiO_2

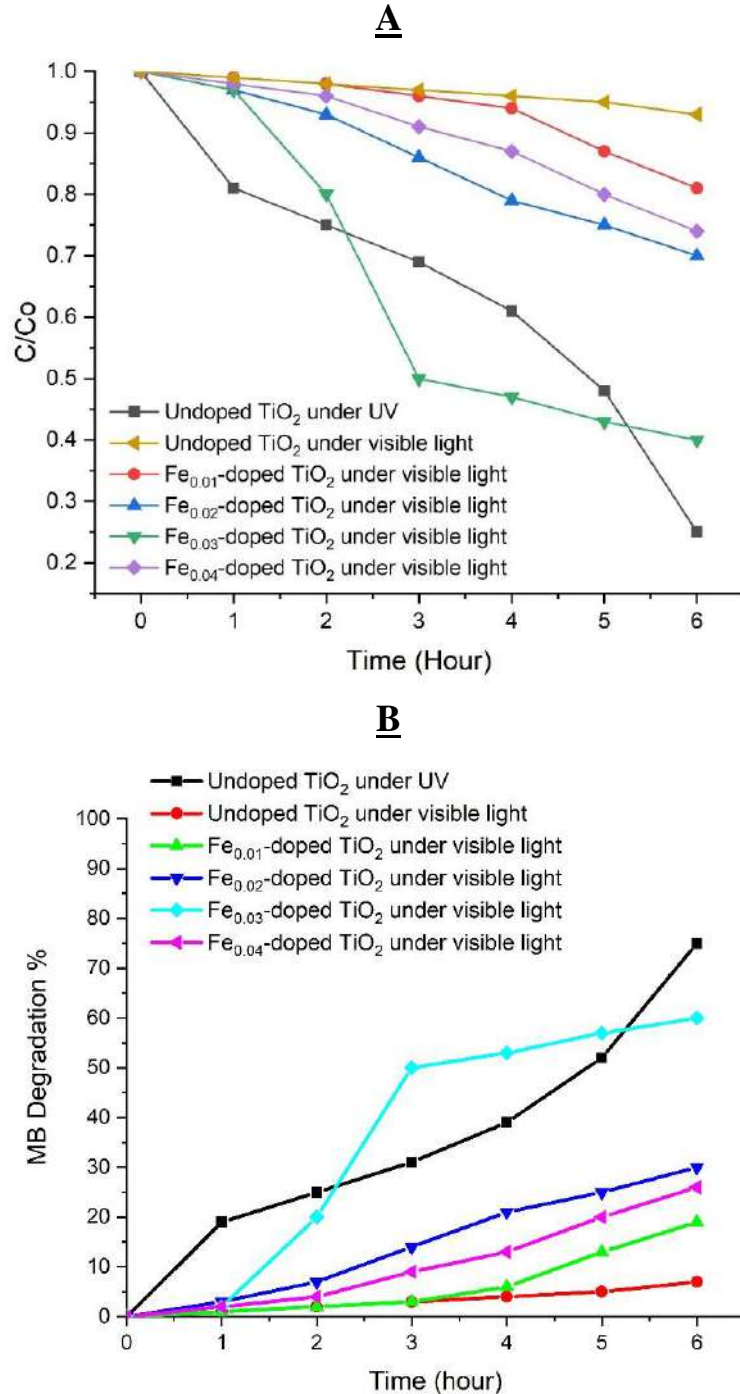


Figure 4.4: Photocatalytic activities of undoped and Fe-doped TiO_2 samples: (A) photocatalytic degradation of MB solution indicated as C/C_0 ($C_0 = 20$ ppm MB solution), (B) MB degradation percentage as a function of irradiation time.

Table 4.4: Photocatalytic Degradation of MB solution


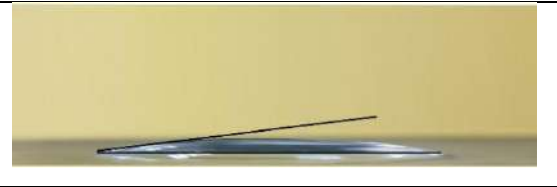
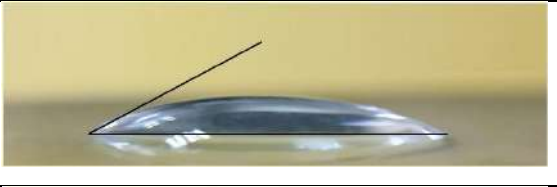
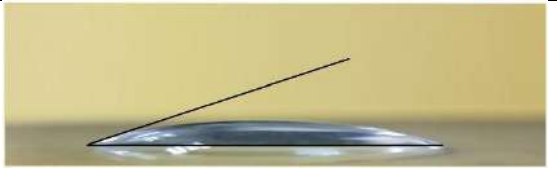
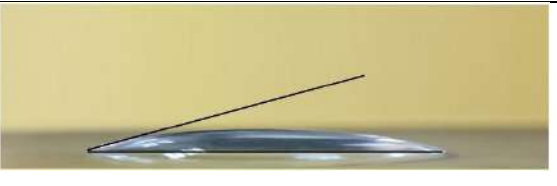
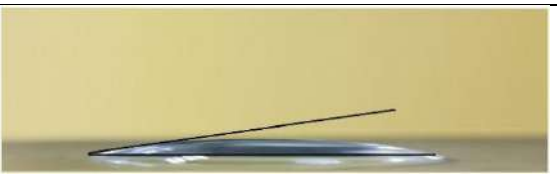
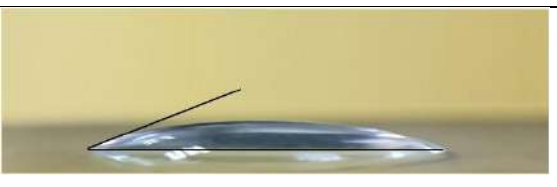
MB Degradation %	After 1 hour	After 2 hour	After 3 hour	After 4 hour	After 5 hour	After 6 hour
Undoped TiO ₂ under UV	19	25	31	39	52	75
Undoped TiO ₂ under visible light	1	2	3	4	5	7
Fe _{0.01} -doped TiO ₂ under visible light	1	2	3	6	13	19
Fe _{0.02} -doped TiO ₂ under visible light	3	7	14	21	25	30
Fe _{0.03} -doped TiO ₂ under visible light	2	20	50	53	57	60
Fe _{0.04} -doped TiO ₂ under visible light	2	4	9	13	20	26

4.5 Hydrophilicity Comparison

Hydrophilicity is the expression of the contact angle of a droplet. To compare the hydrophilicity, the contact angles of the water droplets on the undoped and Fe-doped TiO₂-coated glass surfaces under UV and visible light illumination were measured (**Table 4.5**).

The initial contact angle of the droplet on an uncoated glass surface was 51°. Contact angles of undoped TiO₂-coated glasses under UV and visible light illumination were 7° and 28°, respectively. The obtained result indicates the photocatalytic reaction of undoped TiO₂-coated glass surface under UV light has made it superhydrophilic. As the photocatalytic activity of undoped TiO₂-coated surface under visible light is low, hydrophilicity decreases during visible light illumination.

Table 4.5: Contact angles of the water droplets on the undoped, Fe-doped TiO₂ coated, and uncoated glass surfaces under UV and visible light illumination

Coating type	Contact angle	
Without TiO ₂ coating	51°	
TiO ₂ coating under UV	7°	
TiO ₂ coating under visible light	28°	
Fe _{0.01} -doped TiO ₂ coating under visible light	18°	
Fe _{0.02} -doped TiO ₂ coating under visible light	15°	
Fe _{0.03} -doped TiO ₂ coating under visible light	9°	
Fe _{0.04} -doped TiO ₂ coating under visible light	21°	

Under visible light illumination the contact angles of Fe_{0.01}, Fe_{0.02}, Fe_{0.03} and Fe_{0.04} doped TiO₂ were 18°, 15°, 9° and 21°, respectively. It was also observed that the Fe_{0.03}-doped TiO₂-coated surface showed the best hydrophilicity among Fe-doped TiO₂-coated surfaces as hydrophilicity depends on the photocatalytic reaction of coated surfaces. The findings are consistent and can be correlated with the MB degradation property of Fe-doped TiO₂, where Fe_{0.03}-doped TiO₂ exhibited maximum degradation under the visible region. The competition between the rate transfer of surface charge carriers and the recombination rate of the electrons and holes determines the photocatalytic activity of TiO₂. Oxygen is crucial to this process as it traps electrons in the conduction band and hinders electron-hole recombination [69]. The enhanced photocatalytic reaction of Fe_{0.03}-doped TiO₂-coated surfaces may be explained by the following two parameters.

Particle size effect:

The average particle size and crystallite size of Fe_{0.03}-doped TiO₂ are 21.3 nm and 11.97 nm respectively and are smaller than that of undoped, Fe_{0.01}, Fe_{0.02} doped TiO₂ but larger than that of Fe_{0.04}-doped TiO₂. Ganesh *et al.* explained the fact that nanoparticles having smaller sizes give better photocatalytic reactions [164]. However, the size effect on photocatalytic reaction does not explain the fact for Fe_{0.04}-doped TiO₂.

Effect of band gap reduction and trapping site:

The doped Fe ions form a new energy level below the conduction band and reduce the band gap of TiO₂ by which visible light absorption is possible [69], [167]. The holes and electrons are generated under visible light irradiation. The Fe³⁺ ions work as a trapping site and are able to trap the photoinduced electrons [168]. Because of the reducibility of the photoinduced electrons, the Fe³⁺ ions are reduced to Fe²⁺ ions. Some holes are also trapped by Fe³⁺ to form Fe⁴⁺ ions. The generated Fe²⁺ and Fe⁴⁺ ions are less stable than Fe³⁺ ions. Subsequently, the Fe³⁺ ions appear again by generating hydroxyl radicals ([•]OH) and superoxide (O₂⁻) groups [69], [163]. Fe³⁺ can trap both electrons and holes up to an optimum amount of doping. However, recombination centers can appear if doping

is further increased [168]. This can lead to the reduction of the photo-generated charge carriers resulting in less photocatalytic reaction [163], [169], [170]. In the case of Fe_{0.03}-doped TiO₂, an optimum amount of visible light absorption is observed in which electron and hole trapping sites are increased to an optimum level and electron-hole recombination rate becomes lowest. Thus more ($\cdot\text{OH}$) radicals and (O_2^-) groups are produced. Further increase of Fe content, as in Fe_{0.04}-doped TiO₂, increases electron-hole recombination center, hence the rate of recombination which yields lower photocatalytic reaction and hydrophilicity.

Table 4.6 represents the overall comparison of all the characterizations and tests of the samples. Fe_{0.03}-doped TiO₂ performs better as a photocatalyst under visible light irradiation which yields enhanced photocatalytic reaction and more hydrophilicity.

Table 4.6: Overall comparison of undoped, Fe_{0.01}, Fe_{0.02}, Fe_{0.03}, and Fe_{0.04} doped TiO₂

	Undoped TiO₂	Fe_{0.01} doped TiO₂	Fe_{0.02} doped TiO₂	Fe_{0.03} doped TiO₂	Fe_{0.04} doped TiO₂
Average particle size from SEM (nm)	25.05	23.42	22.39	21.3	20.27
Crystallite size from XRD (nm)	16.67	13.08	12.69	11.97	11.31
Band gap (eV)	3.14	2.52	2.42	2.37	2.25
MB degradation percentage under UV	75	--	--	--	--
MB degradation percentage under visible light	7	19	30	60	26
Contact angle of the droplet under UV	7°	--	--	--	--
Contact angle of the droplet under visible light	28°	18°	15°	9°	21°

CHAPTER 5: CONCLUSIONS AND FUTURE WORK

5.1 Conclusions

Undoped and Fe-doped TiO₂ nanoparticles were synthesized by a simple sol-gel method using tetrabutyl titanate as a precursor and ferric nitrate as an iron doping source. The obtained powder samples were annealed at 500°C to get an anatase structure. XRD patterns of all the samples confirmed 100% anatase phase. The XRD results also revealed that the crystallite size decreases with the increase of Fe doping. The average particle sizes obtained from FESEM analysis and the average crystal sizes obtained from XRD analysis were in a similar pattern. UV-visible spectroscopy analysis indicated that the optical band gap decreases with the increase of Fe doping.

From the photocatalytic dye degradation test, the higher photocatalytic activity (60% MB degradation) under visible light radiation was obtained from Fe_{0.03}-doped TiO₂, having an average particle size of 21.3 nm, average crystallite size of 11.97 nm and band gap of 2.37 eV. Moreover, hydrophilic conversion test also confirmed the enhanced photocatalytic activity for the Fe_{0.03}-doped TiO₂ sample by exhibiting super-hydrophilicity (water droplet contact angle 9°) under visible light radiation. It is worth noting here that the most commonly used indoor LED light was used as the visible light source during the photocatalytic dye degradation and hydrophilic conversion test under the visible region. Though undoped TiO₂ yielded more MB degradation (75%) and super-hydrophilicity (contact angle 7°) than Fe_{0.03}-doped TiO₂ under UV radiation, its photocatalytic activity was very low under visible radiation. Again, the photocatalytic activity of Fe-doped TiO₂ nanoparticles under visible radiation gradually increased with Fe doping till 3 mol% iron concentration. Further increase in Fe doping reduced the photocatalytic activity due to the enhancement of electron-hole recombination rate. As a

result, Fe_{0.04}-doped TiO₂ gave lower MB degradation and lesser hydrophilicity under visible radiation. Hence, in this study optimum range of iron doping concentration was found to be 3 mol% Fe. Therefore, in the sense of photocatalytic activity under visible radiation, Fe_{0.03}-doped TiO₂ performed better as a photocatalyst. Therefore, the iron-doped TiO₂ can be effectively used as self-cleaning coating material.

5.2 Future Work

- In this study, 100% anatase structure for both undoped and Fe-doped TiO₂ nanoparticles was found. The band gap adjustment for visible light sensitization has been carried out only by doping with iron. Developing nanocomposite of TiO₂ with co-doping with other metals, non-metals, and other compounds can be explored to find out future materials with better photocatalytic activity under visible light.
- Photocatalytic water splitting on TiO₂ and platinum electrodes under ultraviolet (UV) light yields hydrogen which can be used as fuel. But, the production of hydrogen as fuel using TiO₂ photocatalyst is not economically efficient. Studies may be carried out in the future to make TiO₂ acceptable for economically efficient hydrogen fuel production.

REFERENCES

- [1] N. Satoh, T. Nakashima, K. Kamikura, and K. Yamamoto, “Quantum Size Effect in TiO₂ Nanoparticles Prepared by Finely Controlled Metal Assembly on Dendrimer Templates,” *Nat. Nanotechnol.*, vol. 3, pp. 106–111, Feb. 2008.
- [2] S. Monticone, R. Tufeu, A. V Kanaev, E. Scolan, and C. Sanchez, “Quantum size effect in TiO₂ nanoparticles: does it exist?,” *Appl. Surf. Sci.*, vol. 162–163, pp. 565–570, 2000.
- [3] M. Anpo, T. Shima, S. Kodama, and Y. Kubokawa, “Photocatalytic hydrogenation of propyne with water on small-particle titania: size quantization effects and reaction intermediates,” *J. Phys. Chem.*, vol. 91, no. 16, pp. 4305–4310, Jul. 1987.
- [4] C. Kormann, D. W. Bahnemann, and M. R. Hoffmann, “Preparation and characterization of quantum-size titanium dioxide,” *J. Phys. Chem.*, vol. 92, no. 18, pp. 5196–5201, Sep. 1988.
- [5] A. Haider, R. Al-Anbari, G. Kadhim, and Z. Jameel, “Synthesis and photocatalytic activity for TiO₂ nanoparticles as air purification,” *MATEC Web Conf.*, vol. 162, pp. 1–6, 2018.
- [6] C. Shuai, C. Shuai, P. Feng, C. Gao, S. Peng, and Y. Yang, “Antibacterial Capability, Physicochemical Properties, and Biocompatibility of nTiO₂ Incorporated Polymeric Scaffolds,” *Polymers*, vol. 10, no. 3. 2018.
- [7] J. Medina-Valtierra, C. Frausto-Reyes, J. Ramírez-Ortiz, and G. Camarillo-Martínez, “Self-Cleaning Test of Doped TiO₂-Coated Glass Plates under Solar Exposure,” *Ind. Eng. Chem. Res.*, vol. 48, no. 2, pp. 598–606, Jan. 2009.
- [8] A. FUJISHIMA and K. HONDA, “Electrochemical Photolysis of Water at a Semiconductor Electrode,” *Nature*, vol. 238, no. 5358, pp. 37–38, 1972.

- [9] J. Zhang, P. Zhou, J. Liu, and J. Yu, “New understanding of the difference of photocatalytic activity among anatase, rutile and brookite TiO₂,” *Phys. Chem. Chem. Phys.*, vol. 16, no. 38, pp. 20382–20386, 2014.
- [10] R. Asahi, T. Morikawa, H. Irie, and T. Ohwaki, “Nitrogen-doped titanium dioxide as visible-light-sensitive photocatalyst: Designs, developments, and prospects,” *Chem. Rev.*, vol. 114, no. 19, pp. 9824–9852, 2014.
- [11] M. Humayun, F. Raziq, A. Khan, and W. Luo, “Modification strategies of TiO₂ for potential applications in photocatalysis: A critical review,” *Green Chem. Lett. Rev.*, vol. 11, no. 2, pp. 86–102, 2018.
- [12] F. Mezzat, H. Zaari, A. Kenz, and A. Benyoussef, “Effect of metal and non metal doping of TiO₂ on photocatalytic activities: ab initio calculations,” *Opt. Quantum Electron.*, vol. 53, Feb. 2021.
- [13] M. Kunnamareddy, R. Rajendran, M. Sivagnanam, R. Rajendran, and B. Diravidamani, “Nickel and sulfur codoped TiO₂ nanoparticles for efficient visible light photocatalytic activity,” *J. Inorg. Organomet. Polym. Mater.*, vol. 31, no. 6, pp. 2615–2626, 2021.
- [14] D. Mane, S. a, S. c, and M. a, *A Review on Metal and Non-metal Doped Titanium Dioxide*, National conference in Chemistry, Shivaji University, Kolhapur, India, 2014.
- [15] V. Moradi, M. B. G. Jun, A. Blackburn, and R. A. Herring, “Significant improvement in visible light photocatalytic activity of Fe doped TiO₂ using an acid treatment process,” *Appl. Surf. Sci.*, vol. 427, pp. 791–799, 2018.
- [16] P. Ragesh, V. Anand Ganesh, S. V. Nair, and A. S. Nair, “A review on ‘self-cleaning and multifunctional materials,’” *J. Mater. Chem. A*, vol. 2, no. 36, pp. 14773–14797, 2014.
- [17] J. Lü *et al.*, “Enhanced photo-induced hydrophilicity of the sol–gel-derived ZnO thin films by Na-doping,” *Appl. Surf. Sci.*, vol. 257, no. 6, pp. 2086–2090, 2011.

- [18] G. K. Hyde *et al.*, “Atomic Layer Deposition and Abrupt Wetting Transitions on Nonwoven Polypropylene and Woven Cotton Fabrics,” *Langmuir*, vol. 26, no. 4, pp. 2550–2558, Feb. 2010.
- [19] M. Miyauchi, A. Nakajima, T. Watanabe, and K. Hashimoto, “Photocatalysis and Photoinduced Hydrophilicity of Various Metal Oxide Thin Films,” *Chem. Mater.*, vol. 14, no. 6, pp. 2812–2816, Jun. 2002.
- [20] I. C. Nica, M. S. Stan, and A. Dinischiotu, “Current photocatalytic applications of nano-scaled titanium dioxide in the new era of " smart " technologies Reviews in Biological and Biomedical Sciences Reviews in Biological and Biomedical Sciences,” vol. 2, no. 1, pp. 1–11, 2019.
- [21] M. Ghanashyam Krishna, M. Vinjanampati, and D. Dhar Purkayastha, “Metal oxide thin films and nanostructures for self-cleaning applications: current status and future prospects,” *Eur. Phys. J. Appl. Phys.*, vol. 62, no. 3, p. 30001, 2013.
- [22] X. T. Zhao, K. Sakka, N. Kihara, Y. Takata, M. Arita, and M. Masuda, “Hydrophilicity of TiO₂ thin films obtained by RF magnetron sputtering deposition,” *Curr. Appl. Phys.*, vol. 6, no. 5, pp. 931–933, Sep. 2006.
- [23] K. Hashimoto, H. Irie, and A. Fujishima, “TiO₂Photocatalysis: A Historical Overview and Future Prospects,” *Jpn. J. Appl. Phys.*, vol. 44, no. 12, pp. 8269–8285, 2005.
- [24] A. Fujishima, X. Zhang, and D. A. Tryk, “TiO₂ photocatalysis and related surface phenomena,” *Surf. Sci. Rep.*, vol. 63, no. 12, pp. 515–582, 2008.
- [25] R. Marschall, “Photocatalysis: Semiconductor Composites: Strategies for Enhancing Charge Carrier Separation to Improve Photocatalytic Activity (Adv. Funct. Mater. 17/2014),” *Adv. Funct. Mater.*, vol. 24, no. 17, p. 2420, May 2014.
- [26] M. Gao, L. Zhu, W. L. Ong, J. Wang, and G. W. Ho, “Structural design of TiO₂-based photocatalyst for H₂ production and degradation applications,” *Catal. Sci. Technol.*, vol. 5, no. 10, pp. 4703–4726, 2015.

- [27] P. Ragesh, V. A. Ganesh, S. V Nair, and A. S. Nair, “FEATURE ARTICLE,” *J. Mater. Chem. A Mater. energy Sustain.*, vol. 2, no. August, pp. 14773–14797, 2014.
- [28] A. N. Approach, *Self-Cleaning Materials*. .
- [29] B. P. Forbes and M. Rubner, “Self-Cleaning Materials: Lotus Leaf-Inspired Nanotechnology: Scientific American Self-Cleaning Materials: Lotus Leaf-Inspired Nanotechnology Self-Cleaning Materials: Lotus Leaf-Inspired Nanotechnology: Scientific American Page 2 of 5,” pp. 1–5, 2008.
- [30] S. Greßler, U. Fiedeler, and M. Simkó, “Self-cleaning , dirt and water-repellent coatings on the basis of nanotechnology,” vol. 2, no. November 2015, 2010.
- [31] D. Vollath, “Nanomaterials an introduction to synthesis, properties and application ,” *Environ. Eng. Manag. Journal; Vol 7, No 6*, 2008.
- [32] G. Lidén, “The European Commission Tries to Define Nanomaterials,” *Ann. Occup. Hyg.*, vol. 55, no. 1, pp. 1–5, Jan. 2011.
- [33] N. Baig, I. Kammakakam, and W. Falath, “Nanomaterials: a review of synthesis methods, properties, recent progress, and challenges,” *Mater. Adv.*, vol. 2, no. 6, pp. 1821–1871, 2021.
- [34] R. Jose Varghese, E. hadji M. Sakho, S. Parani, S. Thomas, O. S. Oluwafemi, and J. Wu, “Chapter 3 - Introduction to nanomaterials: synthesis and applications,” S. Thomas, E. H. M. Sakho, N. Kalarikkal, S. O. Oluwafemi, and J. B. T.-N. for S. C. A. Wu, Eds. Elsevier, 2019, pp. 75–95.
- [35] A. Husen, “Chapter 1 - Introduction and techniques in nanomaterials formulation,” in *Micro and Nano Technologies*, A. Husen and M. B. T.-N. for A. and F. A. Jawaid, Eds. Elsevier, 2020, pp. 1–14.
- [36] A. B. Asha and R. Narain, “Chapter 15 - Nanomaterials properties,” R. B. T.-P. S. and N. Narain, Ed. Elsevier, 2020, pp. 343–359.

- [37] J. G. Muga, “Quantum Theory of Tunneling,” *Phys. Today*, vol. 57, no. 2, pp. 66–67, Feb. 2004.
- [38] L. J. Lauhon and W. Ho, “Direct Observation of the Quantum Tunneling of Single Hydrogen Atoms with a Scanning Tunneling Microscope,” *Phys. Rev. Lett.*, vol. 85, no. 21, pp. 4566–4569, Nov. 2000.
- [39] Q. Smets *et al.*, “InGaAs tunnel diodes for the calibration of semi-classical and quantum mechanical band-to-band tunneling models,” *J. Appl. Phys.*, vol. 115, no. 18, p. 184503, May 2014.
- [40] S. Sorcar, “SYNTHESIS AND STUDY OF CATION DOPED TITANIUM,” no. July 2014, 2016.
- [41] J. Connerade, “A Review of Quantum Confinement,” *AIP Conf. Proc.*, vol. 1197, no. 1, pp. 1–33, Dec. 2009.
- [42] R. Koole, E. Groeneveld, D. Vanmaekelbergh, A. Meijerink, and C. de Mello Donegá, “Size Effects on Semiconductor Nanoparticles BT - Nanoparticles: Workhorses of Nanoscience,” C. de Mello Donegá, Ed. Berlin, Heidelberg: Springer Berlin Heidelberg, 2014, pp. 13–51.
- [43] S. Mohan Bhagyaraj and O. S. Oluwafemi, “Chapter 1 - Nanotechnology: The Science of the Invisible,” in *Micro and Nano Technologies*, S. Mohan Bhagyaraj, O. S. Oluwafemi, N. Kalarikkal, and S. B. T.-S. of I. N. Thomas, Eds. Woodhead Publishing, 2018, pp. 1–18.
- [44] M. Le Goas *et al.*, “How Do Surface Properties of Nanoparticles Influence Their Diffusion in the Extracellular Matrix? A Model Study in Matrigel Using Polymer-Grafted Nanoparticles,” *Langmuir*, vol. 36, no. 35, pp. 10460–10470, Sep. 2020.
- [45] I. Khan, K. Saeed, and I. Khan, “Nanoparticles: Properties, applications and toxicities,” *Arab. J. Chem.*, vol. 12, no. 7, pp. 908–931, 2019.
- [46] M. G. Lines, “Nanomaterials for practical functional uses,” *J. Alloys Compd.*, vol.

449, no. 1, pp. 242–245, 2008.

- [47] B. Carl Englert, “Nanomaterials and the environment: uses, methods and measurement,” *J. Environ. Monit.*, vol. 9, no. 11, pp. 1154–1161, 2007.
- [48] E. Garbayo, A. Estella-Hermoso de Mendoza, and M. J. Blanco-Prieto, “Diagnostic and Therapeutic Uses of Nanomaterials in the Brain,” *Current Medicinal Chemistry*, vol. 21, no. 36, pp. 4100–4131.
- [49] K. I. Hadjiivanov and D. G. Klissurski, “Surface chemistry of titania (anatase) and titania-supported catalysts,” *Chem. Soc. Rev.*, vol. 25, no. 1, pp. 61–69, 1996.
- [50] A. Heller, “Chemistry and Applications of Photocatalytic Oxidation of Thin Organic Films,” *Acc. Chem. Res.*, vol. 28, no. 12, pp. 503–508, Dec. 1995.
- [51] A. L. Linsebigler, G. Lu, and J. T. Yates, “Photocatalysis on TiO₂ Surfaces: Principles, Mechanisms, and Selected Results,” *Chem. Rev.*, vol. 95, no. 3, pp. 735–758, May 1995.
- [52] S. Yang, N. Huang, Y. M. Jin, H. Q. Zhang, Y. H. Su, and H. G. Yang, “Crystal shape engineering of anatase TiO₂ and its biomedical applications,” *CrystEngComm*, vol. 17, no. 35, pp. 6617–6631, 2015.
- [53] G. Cangiani, A. Baldereschi, M. Posternak, and H. Krakauer, “Born charge differences of TiO₂ polytypes: Multipole expansion of Wannier charge densities,” *Phys. Rev. B*, vol. 69, no. 12, p. 121101, Mar. 2004.
- [54] Y. Zhang, W. Lin, Y. Li, K. Ding, and J. Li, “A Theoretical Study on the Electronic Structures of TiO₂: Effect of Hartree–Fock Exchange,” *J. Phys. Chem. B*, vol. 109, no. 41, pp. 19270–19277, Oct. 2005.
- [55] R. Asahi, Y. Taga, W. Mannstadt, and A. J. Freeman, “Electronic and optical properties of anatase TiO₂,” *Phys. Rev. B*, vol. 61, no. 11, pp. 7459–7465, Mar. 2000.
- [56] P. I. Sorantin and K. Schwarz, “Chemical bonding in rutile-type compounds,”

Inorg. Chem., vol. 31, no. 4, pp. 567–576, Feb. 1992.

- [57] S. G. Kumar and K. S. R. K. Rao, “Polymorphic phase transition among the titania crystal structures using a solution-based approach: From precursor chemistry to nucleation process,” *Nanoscale*, vol. 6, no. 20, pp. 11574–11632, 2014.
- [58] R. Asahi, T. Morikawa, T. Ohwaki, K. Aoki, and Y. Taga, “Visible-Light Photocatalysis in Nitrogen-Doped Titanium Oxides,” *Science (80-.)*, vol. 293, no. 5528, pp. 269–271, Jul. 2001.
- [59] H. Irie, Y. Watanabe, and K. Hashimoto, “Nitrogen-Concentration Dependence on Photocatalytic Activity of TiO₂-xN_x Powders,” *J. Phys. Chem. B*, vol. 107, no. 23, pp. 5483–5486, Jun. 2003.
- [60] T. Ihara, M. Miyoshi, Y. Iriyama, O. Matsumoto, and S. Sugihara, “Visible-light-active titanium oxide photocatalyst realized by an oxygen-deficient structure and by nitrogen doping,” *Appl. Catal. B Environ.*, vol. 42, no. 4, pp. 403–409, 2003.
- [61] Z. Zhao and Q. Liu, “Mechanism of higher photocatalytic activity of anatase TiO₂ doped with nitrogen under visible-light irradiation from density functional theory calculation,” *J. Phys. D. Appl. Phys.*, vol. 41, no. 2, 2008.
- [62] M. R. Hoffmann, S. T. Martin, W. Choi, and D. W. Bahnemann, “Environmental Applications of Semiconductor Photocatalysis,” *Chem. Rev.*, vol. 95, no. 1, pp. 69–96, Jan. 1995.
- [63] Y. Zhang, H. Shen, and Y. Liu, “Cooperation between N and Fe in co-doped TiO₂ photocatalyst,” *Res. Chem. Intermed.*, vol. 42, no. 2, pp. 687–711, 2016.
- [64] T. Tong, J. Zhang, B. Tian, F. Chen, and D. He, “Preparation of Fe³⁺-doped TiO₂ catalysts by controlled hydrolysis of titanium alkoxide and study on their photocatalytic activity for methyl orange degradation,” *J. Hazard. Mater.*, vol. 155, no. 3, pp. 572–579, 2008.

- [65] X. Yan, C. Xue, B. Yang, and G. Yang, “Novel three-dimensionally ordered macroporous Fe³⁺-doped TiO₂ photocatalysts for H₂ production and degradation applications,” *Appl. Surf. Sci.*, vol. 394, pp. 248–257, 2017.
- [66] M. Zhou, J. Yu, and B. Cheng, “Effects of Fe-doping on the photocatalytic activity of mesoporous TiO₂ powders prepared by an ultrasonic method,” *J. Hazard. Mater.*, vol. 137, no. 3, pp. 1838–1847, 2006.
- [67] R. da S. Santos *et al.*, “Iron Insertion and Hematite Segregation on Fe-Doped TiO₂ Nanoparticles Obtained from Sol–Gel and Hydrothermal Methods,” *ACS Appl. Mater. Interfaces*, vol. 4, no. 10, pp. 5555–5561, Oct. 2012.
- [68] S. Tieng, R. Azouani, K. Chhor, and A. Kanaev, “Nucleation–Growth of TiO₂ Nanoparticles Doped with Iron Acetylacetonate,” *J. Phys. Chem. C*, vol. 115, no. 13, pp. 5244–5250, Apr. 2011.
- [69] M. B. Marami, M. Farahmandjou, and B. Khoshnevisan, “Sol–Gel Synthesis of Fe-Doped TiO₂ Nanocrystals,” *J. Electron. Mater.*, vol. 47, no. 7, pp. 3741–3748, 2018.
- [70] G. Sadanandam, L. Zhang, and M. S. Scurrall, “Enhanced photocatalytic hydrogen formation over Fe-loaded TiO₂ and g-C₃N₄ composites from mixed glycerol and water by solar irradiation,” *J. Renew. Sustain. Energy*, vol. 10, no. 3, p. 34703, May 2018.
- [71] T. H. Kim, V. Rodríguez-González, G. Gyawali, S. H. Cho, T. Sekino, and S. W. Lee, “Synthesis of solar light responsive Fe, N co-doped TiO₂ photocatalyst by sonochemical method,” *Catal. Today*, vol. 212, pp. 75–80, 2013.
- [72] P. Yu, S. S. Wang, H. H. Li, and W. X. Li, “N, Fe Co-Doped TiO₂ Photocatalyst Preparation by Sol-Gel Method with Visible Light Response,” in *Advanced Materials Research*, 2013, vol. 726, pp. 673–676.
- [73] I. C. Nica *et al.*, “Innovative self-cleaning and biocompatible polyester textiles nano-decorated with Fe-N-doped titanium dioxide,” *Nanomaterials*, vol. 6, no.

11, 2016.

- [74] R. Jothi Ramalingam, P. Arunachalam, T. Radhika, K. R. Anju, K. C. Nimitha, and H. A. Al-Lohedan, "Surface and electrochemical characterization of N-Fe-doped-TiO₂ nanoparticle prepared by hydrothermal and facile electro-deposition method for visible light driven pollutant removal," *Int. J. Electrochem. Sci.*, vol. 12, no. 1, pp. 797–811, 2017.
- [75] S. Larumbe, M. Monge, and C. Gómez-Polo, "Comparative study of (N, Fe) doped TiO₂ photocatalysts," *Appl. Surf. Sci.*, vol. 327, pp. 490–497, 2015.
- [76] T. Ohwaki, S. Saeki, K. Aoki, and T. Morikawa, "Evaluation of photocatalytic activities and characteristics of Cu- or Fe-modified nitrogen-doped titanium dioxides for applications in environmental purification," *Jpn. J. Appl. Phys.*, vol. 55, no. 1S, p. 01AA05, 2015.
- [77] X. Li, Z. Chen, Y. Shi, and Y. Liu, "Preparation of N, Fe co-doped TiO₂ with visible light response," *Powder Technol.*, vol. 207, no. 1–3, pp. 165–169, 2011.
- [78] K. Zhang, X. Wang, X. Guo, T. He, and Y. Feng, "Preparation of highly visible light active Fe–N co-doped mesoporous TiO₂ photocatalyst by fast sol–gel method," *J. Nanoparticle Res.*, vol. 16, no. 2, p. 2246, 2014.
- [79] N. K. A.-N. K. A.-S. K. S. A.-V. Singh, "Synthesis, characterization and photocatalytic activity of magnetically separable γ -Fe₂O₃/N,Fe codoped TiO₂ heterojunction for degradation of Reactive Blue 4 dye," *RSC Adv.*, vol. v. 5, no. 76, pp. 61623-61630–2015 v.5 no.76, 2015.
- [80] D. Vione, C. Minero, V. Maurino, M. E. Carlotti, T. Picatonotto, and E. Pelizzetti, "Degradation of phenol and benzoic acid in the presence of a TiO₂-based heterogeneous photocatalyst," *Appl. Catal. B Environ.*, vol. 58, no. 1, pp. 79–88, 2005.
- [81] K. Pirkanniemi and M. Sillanpää, "Heterogeneous water phase catalysis as an environmental application: A review," *Chemosphere*, vol. 48, no. 10, pp. 1047–

1060, 2002.

- [82] S. Malato, J. Blanco, A. Vidal, and C. Richter, "Photocatalysis with solar energy at a pilot-plant scale: An overview," *Appl. Catal. B Environ.*, vol. 37, no. 1, pp. 1–15, 2002.
- [83] Y. Bessekhoud, D. Robert, J. V. Weber, and N. Chaoui, "Effect of alkaline-doped TiO₂ on photocatalytic efficiency," *J. Photochem. Photobiol. A Chem.*, vol. 167, no. 1, pp. 49–57, 2004.
- [84] S. Malato, J. Blanco, J. Cáceres, A. R. Fernández-Alba, A. Agüera, and A. Rodríguez, "Photocatalytic treatment of water-soluble pesticides by photo-Fenton and TiO₂ using solar energy," *Catal. Today*, vol. 76, no. 2–4, pp. 209–220, 2002.
- [85] M. V. Phanikrishna Sharma, V. Durga Kumari, and M. Subrahmanyam, "TiO₂ supported over SBA-15: An efficient photocatalyst for the pesticide degradation using solar light," *Chemosphere*, vol. 73, no. 9, pp. 1562–1569, 2008.
- [86] I. K. Konstantinou and T. A. Albanis, "Photocatalytic transformation of pesticides in aqueous titanium dioxide suspensions using artificial and solar light: Intermediates and degradation pathways," *Appl. Catal. B Environ.*, vol. 42, no. 4, pp. 319–335, 2003.
- [87] N. Daneshvar, S. Aber, M. S. Seyed Dorraji, A. R. Khataee, and M. H. Rasoulifard, "Photocatalytic degradation of the insecticide diazinon in the presence of prepared nanocrystalline ZnO powders under irradiation of UV-C light," *Sep. Purif. Technol.*, vol. 58, no. 1, pp. 91–98, 2007.
- [88] A. A. Adesina, "Industrial exploitation of photocatalysis: Progress, perspectives and prospects," *Catal. Surv. from Asia*, vol. 8, no. 4, pp. 265–273, 2004.
- [89] V. Brezová *et al.*, "Phenol decomposition using Mn⁺/TiO₂ photocatalysts supported by the sol-gel technique on glass fibres," *J. Photochem. Photobiol. A Chem.*, vol. 109, no. 2, pp. 177–183, 1997.

- [90] H. Ling, K. Kim, Z. Liu, J. Shi, X. Zhu, and J. Huang, "Photocatalytic degradation of phenol in water on as-prepared and surface modified TiO₂ nanoparticles," *Catal. Today*, vol. 258, pp. 96–102, 2015.
- [91] X. Hao, M. Li, L. Zhang, K. Wang, and C. Liu, "Photocatalyst TiO₂/WO₃/GO nano-composite with high efficient photocatalytic performance for BPA degradation under visible light and solar light illumination," *J. Ind. Eng. Chem.*, vol. 55, pp. 140–148, 2017.
- [92] D. Khamboonrueang, S. Srirattanapibul, I. M. Tang, and S. Thongmee, "TiO₂-rGO nanocomposite as a photo catalyst for the reduction of Cr⁶⁺," *Mater. Res. Bull.*, vol. 107, no. April, pp. 236–241, 2018.
- [93] H.-T. Ren, S.-Y. Jia, J.-J. Zou, S.-H. Wu, and X. Han, "A facile preparation of Ag₂O/P25 photocatalyst for selective reduction of nitrate," *Appl. Catal. B Environ.*, vol. 176–177, pp. 53–61, 2015.
- [94] C. Fan *et al.*, "Black Hydroxylated Titanium Dioxide Prepared via Ultrasonication with Enhanced Photocatalytic Activity," *Nat. Publ. Gr.*, no. September 2014, pp. 1–10, 2015.
- [95] J. Lyu, L. Zhu, and C. Burda, "Considerations to improve adsorption and photocatalysis of low concentration air pollutants on TiO₂," *Catal. Today*, vol. 225, pp. 24–33, 2014.
- [96] B. S. Rodrigues, K. T. Ranjit, S. Uma, I. N. Martyanov, and K. J. Klabunde, "Single-Step Synthesis of a Highly Active Visible-Light Photocatalyst for Oxidation of a Common Indoor Air Pollutant : Acetaldehyde **," pp. 2467–2471, 2005.
- [97] K. Fujiwara, U. Müller, and S. E. Pratsinis, "Pd Subnano-Clusters on TiO₂ for Solar-Light Removal of NO," *ACS Catal.*, vol. 6, no. 3, pp. 1887–1893, Mar. 2016.
- [98] N. C. T. Martins, J. Ângelo, A. V. Girão, T. Trindade, L. Andrade, and A.

- Mendes, “N-doped carbon quantum dots/TiO₂ composite with improved photocatalytic activity,” *Appl. Catal. B Environ.*, vol. 193, pp. 67–74, 2016.
- [99] L. Zeng, W. Song, M. Li, D. Zeng, and C. Xie, “Catalytic oxidation of formaldehyde on surface of HTiO₂/HCTiO₂ without light illumination at room temperature,” *Appl. Catal. B Environ.*, vol. 147, pp. 490–498, 2014.
- [100] M. D. Hernández-Alonso, I. Tejedor-Tejedor, J. M. Coronado, M. A. Anderson, and J. Soria, “Operando FTIR study of the photocatalytic oxidation of acetone in air over TiO₂–ZrO₂ thin films,” *Catal. Today*, vol. 143, no. 3, pp. 364–373, 2009.
- [101] Y. Xu, Y. Zhuang, and X. Fu, “New Insight for Enhanced Photocatalytic Activity of TiO₂ by Doping Carbon Nanotubes: A Case Study on Degradation of Benzene and Methyl Orange,” pp. 2669–2676, 2010.
- [102] X. Kang, X. Z. Song, Y. Han, J. Cao, and Z. Tan, “Defect-engineered TiO₂ Hollow Spiny Nanocubes for Phenol Degradation under Visible Light Irradiation,” *Sci. Rep.*, vol. 8, no. 1, pp. 1–10, 2018.
- [103] S. Yamazaki, H. Tsukamoto, K. Araki, T. Tanimura, I. Tejedor-Tejedor, and M. A. Anderson, “Photocatalytic degradation of gaseous tetrachloroethylene on porous TiO₂ pellets,” *Appl. Catal. B Environ.*, vol. 33, no. 2, pp. 109–117, 2001.
- [104] S. Ahmed, M. G. Rasul, R. Brown, and M. A. Hashib, “Influence of parameters on the heterogeneous photocatalytic degradation of pesticides and phenolic contaminants in wastewater: A short review,” *J. Environ. Manage.*, vol. 92, no. 3, pp. 311–330, 2011.
- [105] K. M. Parida, N. Sahu, N. R. Biswal, B. Naik, and A. C. Pradhan, “Preparation, characterization, and photocatalytic activity of sulfate-modified titania for degradation of methyl orange under visible light,” *J. Colloid Interface Sci.*, vol. 318, no. 2, pp. 231–237, 2008.
- [106] H. Guan, D. Chi, J. Yu, and X. Li, “A novel photodegradable insecticide: Preparation, characterization and properties evaluation of nano-Imidacloprid,”

Pestic. Biochem. Physiol., vol. 92, no. 2, pp. 83–91, 2008.

- [107] G. Aragay, F. Pino, and A. Merkoçi, “Nanomaterials for sensing and destroying pesticides,” *Chem. Rev.*, vol. 112, no. 10, pp. 5317–5338, 2012.
- [108] S. Devipriya and S. Yesodharan, “Photocatalytic degradation of pesticide contaminants in water,” *Sol. Energy Mater. Sol. Cells*, vol. 86, no. 3, pp. 309–348, 2005.
- [109] K. Lee, H. Ku, and D. Pak, “OH radical generation in a photocatalytic reactor using TiO₂ nanotube plates,” *Chemosphere*, vol. 149, pp. 114–120, 2016.
- [110] S. Rabindranathan, S. Devipriya, and S. Yesodharan, “Photocatalytic degradation of phosphamidon on semiconductor oxides,” *J. Hazard. Mater.*, vol. 102, no. 2–3, pp. 217–229, 2003.
- [111] L. Lhomme, S. Brosillon, and D. Wolbert, “Photocatalytic degradation of pesticides in pure water and a commercial agricultural solution on TiO₂ coated media,” *Chemosphere*, vol. 70, no. 3, pp. 381–386, 2008.
- [112] N. Attarchi, M. Montazer, and T. Toliyat, “Ag/TiO₂/β-CD nano composite: Preparation and photo catalytic properties for methylene blue degradation,” *Appl. Catal. A Gen.*, vol. 467, pp. 107–116, 2013.
- [113] S. Bzdon, J. Góralski, W. Maniukiewicz, J. Perkowski, J. Rogowski, and M. Szadkowska-Nicze, “Radiation-induced synthesis of Fe-doped TiO₂: Characterization and catalytic properties,” *Radiat. Phys. Chem.*, vol. 81, no. 3, pp. 322–330, 2012.
- [114] M. A. M. L. de Jesus, J. T. da S. Neto, G. Timò, P. R. P. Paiva, M. S. S. Dantas, and A. de M. Ferreira, “Superhydrophilic self-cleaning surfaces based on TiO₂ and TiO₂/SiO₂ composite films for photovoltaic module cover glass,” *Appl. Adhes. Sci.*, vol. 3, no. 1, p. 5, 2015.
- [115] M. Yamamoto *et al.*, “Theoretical Explanation of the Lotus Effect:

- Superhydrophobic Property Changes by Removal of Nanostructures from the Surface of a Lotus Leaf,” *Langmuir*, vol. 31, no. 26, pp. 7355–7363, Jul. 2015.
- [116] A. Mills, A. Lepre, N. Elliott, S. Bhopal, I. P. Parkin, and S. A. O’Neill, “Characterisation of the photocatalyst Pilkington ActivTM: a reference film photocatalyst?,” *J. Photochem. Photobiol. A Chem.*, vol. 160, no. 3, pp. 213–224, 2003.
- [117] H. Honda, A. Ishizaki, R. Soma, K. Hashimoto, and A. Fujishima, “Application of Photocatalytic Reactions Caused by TiO₂ Film to Improve the Maintenance Factor of Lighting Systems,” *J. Illum. Eng. Soc.*, vol. 27, no. 1, pp. 42–49, 1998.
- [118] D. Synnott, N. Nolan, D. Ryan, J. Colreavy, and S. C. Pillai, “14 - Self-cleaning tiles and glasses for eco-efficient buildings,” in *Nanotechnology in Eco-Efficient Construction*, F. Pacheco-Torgal, M. V Diamanti, A. Nazari, and C.-G. Granqvist, Eds. Woodhead Publishing, 2013, pp. 327–342.
- [119] S. Banerjee, D. D. Dionysiou, and S. C. Pillai, “Self-cleaning applications of TiO₂ by photo-induced hydrophilicity and photocatalysis,” *Appl. Catal. B Environ.*, vol. 176–177, pp. 396–428, 2015.
- [120] J. Mo, Y. Zhang, Q. Xu, J. Joaquin, and R. Zhao, “Photocatalytic purification of volatile organic compounds in indoor air: A literature review,” *Atmos. Environ.*, vol. 43, no. 14, pp. 2229–2246, 2009.
- [121] X. Chen and S. S. Mao, “Titanium Dioxide Nanomaterials: Synthesis, Properties, Modifications, and Applications,” *Chem. Rev.*, vol. 107, no. 7, pp. 2891–2959, Jul. 2007.
- [122] W. A. Jacoby, P. C. Maness, E. J. Wolfrum, D. M. Blake, and J. A. Fennell, “Mineralization of Bacterial Cell Mass on a Photocatalytic Surface in Air,” *Environ. Sci. Technol.*, vol. 32, no. 17, pp. 2650–2653, Sep. 1998.
- [123] X. Chen, C. Li, M. Grätzel, R. Kostecki, and S. S. Mao, “Nanomaterials for renewable energy production and storage,” *Chem. Soc. Rev.*, vol. 41, no. 23, pp.

7909–7937, 2012.

- [124] G. L. Chiarello, M. V. Dozzi, and E. Selli, “TiO₂-based materials for photocatalytic hydrogen production,” *J. Energy Chem.*, vol. 26, no. 2, pp. 250–258, 2017.
- [125] X. Zou, J. Liu, J. Su, F. Zuo, J. Chen, and P. Feng, “Facile Synthesis of Thermal- and Photostable Titania with Paramagnetic Oxygen Vacancies for Visible-Light Photocatalysis,” *Chem. – A Eur. J.*, vol. 19, no. 8, pp. 2866–2873, 2013.
- [126] W. Zhou *et al.*, “Ordered Mesoporous Black TiO₂ as Highly Efficient Hydrogen Evolution Photocatalyst,” *J. Am. Chem. Soc.*, vol. 136, no. 26, pp. 9280–9283, Jul. 2014.
- [127] R. Zhong *et al.*, “Covalently bonded 2D/2D O-g-C₃N₄/TiO₂ heterojunction for enhanced visible-light photocatalytic hydrogen evolution,” *Appl. Catal. B Environ.*, vol. 237, pp. 1130–1138, 2018.
- [128] Slamet, H. W. Nasution, E. Purnama, S. Kosela, and J. Gunlazuardi, “Photocatalytic reduction of CO₂ on copper-doped Titania catalysts prepared by improved-impregnation method,” *Catal. Commun.*, vol. 6, no. 5, pp. 313–319, 2005.
- [129] D. Liu *et al.*, “On the impact of Cu dispersion on CO₂ photoreduction over Cu/TiO₂,” *Catal. Commun.*, vol. 25, pp. 78–82, 2012.
- [130] G. Liu *et al.*, “Study on a stretchable, fiber-shaped, and TiO₂ nanowire array-based dye-sensitized solar cell with electrochemical impedance spectroscopy method,” *Electrochim. Acta*, vol. 267, pp. 34–40, 2018.
- [131] B. Liu *et al.*, “Branched hierarchical photoanode of anatase TiO₂ nanotubes on rutile TiO₂ nanorod arrays for efficient quantum dot-sensitized solar cells,” *J. Mater. Chem. A*, vol. 3, no. 8, pp. 4445–4452, 2015.
- [132] J. Chen *et al.*, “C@TiO₂ nanocomposites with impressive electrochemical

- performances as anode material for lithium-ion batteries,” *J. Alloys Compd.*, vol. 742, pp. 828–834, 2018.
- [133] D. Su, S. Dou, and G. Wang, “Anatase TiO₂: Better Anode Material Than Amorphous and Rutile Phases of TiO₂ for Na-Ion Batteries,” *Chem. Mater.*, vol. 27, no. 17, pp. 6022–6029, Sep. 2015.
- [134] C. Kim, S. Kim, J. Lee, J. Kim, and J. Yoon, “Capacitive and Oxidant Generating Properties of Black-Colored TiO₂ Nanotube Array Fabricated by Electrochemical Self-Doping,” *ACS Appl. Mater. Interfaces*, vol. 7, no. 14, pp. 7486–7491, Apr. 2015.
- [135] L. Wang, C. Hu, and L. Shao, “The antimicrobial activity of nanoparticles: present situation and prospects for the future,” *Int. J. Nanomedicine*, vol. 12, pp. 1227–1249, Feb. 2017.
- [136] Galib, M. Barve, M. Mashru, C. Jagtap, B. J. Patgiri, and P. K. Prajapati, “Therapeutic potentials of metals in ancient India: A review through Charaka Samhita,” *J. Ayurveda Integr. Med.*, vol. 2, no. 2, pp. 55–63, Apr. 2011.
- [137] Y. Gong, C. Li, Y. Zhang, and D. Gong, “Discovery of ancient mineral medicine in the Lv family tomb of the Northern Song dynasty (1074–1111 ce),” *Archaeometry*, vol. 61, no. 2, pp. 442–449, 2019.
- [138] J. T. Seil and T. J. Webster, “Antimicrobial applications of nanotechnology: methods and literature,” *Int. J. Nanomedicine*, vol. 7, pp. 2767–2781, 2012.
- [139] K. Hirakawa, M. Mori, M. Yoshida, S. Oikawa, and S. Kawanishi, “Photo-irradiated titanium dioxide catalyzes site specific DNA damage via generation of hydrogen peroxide,” *Free Radic. Res.*, vol. 38, no. 5, pp. 439–447, 2004.
- [140] A. Sirelkhatim *et al.*, “Review on zinc oxide nanoparticles: Antibacterial activity and toxicity mechanism,” *Nano-Micro Lett.*, vol. 7, no. 3, pp. 219–242, 2015.
- [141] A. R. Shahverdi, A. Fakhimi, H. R. Shahverdi, and S. Minaian, “Synthesis and

- effect of silver nanoparticles on the antibacterial activity of different antibiotics against *Staphylococcus aureus* and *Escherichia coli*,” *Nanomedicine Nanotechnology, Biol. Med.*, vol. 3, no. 2, pp. 168–171, 2007.
- [142] J. Karlsson, S. Atefyekta, and M. Andersson, “Controlling drug delivery kinetics from mesoporous titania thin films by pore size and surface energy,” *Int. J. Nanomedicine*, vol. 10, pp. 4425–4436, Jul. 2015.
- [143] B. Gupta *et al.*, “Hyaluronic acid-capped compact silica-supported mesoporous titania nanoparticles for ligand-directed delivery of doxorubicin,” *Acta Biomater.*, vol. 80, pp. 364–377, 2018.
- [144] Z. Guo *et al.*, “Overcoming drug resistance with functional mesoporous titanium dioxide nanoparticles combining targeting, drug delivery and photodynamic therapy,” *J. Mater. Chem. B*, vol. 6, no. 46, pp. 7750–7759, 2018.
- [145] M. Nakayama *et al.*, “Titanium peroxide nanoparticles enhanced cytotoxic effects of X-ray irradiation against pancreatic cancer model through reactive oxygen species generation in vitro and in vivo,” *Radiat. Oncol.*, vol. 11, no. 1, p. 91, 2016.
- [146] Z. Dai *et al.*, “Dual-stimuli-responsive TiO_x/DOX nanodrug system for lung cancer synergistic therapy,” *RSC Adv.*, vol. 8, no. 39, pp. 21975–21984, 2018.
- [147] P. Wu, R. Xie, J. A. Imlay, and J. K. Shang, “Visible-Light-Induced Photocatalytic Inactivation of Bacteria by Composite Photocatalysts of Palladium Oxide and Nitrogen-Doped Titanium Oxide,” *Appl. Catal. B.*, vol. 88, no. 3–4, pp. 576–581, May 2009.
- [148] R. Bagherzadeh, M. Montazer, M. Latifi, M. Sheikhzadeh, and M. Sattari, “Evaluation of comfort properties of polyester knitted spacer fabrics finished with water repellent and antimicrobial agents,” *Fibers Polym.*, vol. 8, no. 4, pp. 386–392, 2007.
- [149] D. C. Davis, J. W. Wilkerson, J. Zhu, and V. G. Hadjiev, “A strategy for

- improving mechanical properties of a fiber reinforced epoxy composite using functionalized carbon nanotubes,” *Compos. Sci. Technol.*, vol. 71, no. 8, pp. 1089–1097, 2011.
- [150] M. Gorenšek and P. Recelj, “Nanosilver Functionalized Cotton Fabric,” *Text. Res. J.*, vol. 77, no. 3, pp. 138–141, Mar. 2007.
- [151] S. Mondal and J. L. Hu, “A novel approach to excellent UV protecting cotton fabric with functionalized MWNT containing water vapor permeable PU coating,” *J. Appl. Polym. Sci.*, vol. 103, no. 5, pp. 3370–3376, Mar. 2007.
- [152] N. Abidi, L. Cabrales, and E. Hequet, “Functionalization of a Cotton Fabric Surface with Titania Nanosols: Applications for Self-Cleaning and UV-Protection Properties,” *ACS Appl. Mater. Interfaces*, vol. 1, no. 10, pp. 2141–2146, Oct. 2009.
- [153] S. Afzal, W. A. Daoud, and S. J. Langford, “Photostable Self-Cleaning Cotton by a Copper(II) Porphyrin/TiO₂ Visible-Light Photocatalytic System,” *ACS Appl. Mater. Interfaces*, vol. 5, no. 11, pp. 4753–4759, Jun. 2013.
- [154] E. Pakdel, W. A. Daoud, T. Afrin, L. Sun, and X. Wang, “Self-cleaning wool: effect of noble metals and silica on visible-light-induced functionalities of nano TiO₂ colloid,” *J. Text. Inst.*, vol. 106, no. 12, pp. 1348–1361, Dec. 2015.
- [155] Y. L. Lam, C. W. Kan, and C. W. M. Yuen, “Effect of concentration of titanium dioxide acting as catalyst or co-catalyst on the wrinkle-resistant finishing of cotton fabric,” *Fibers Polym.*, vol. 11, no. 4, pp. 551–558, 2010.
- [156] D. Pasqui and R. Barbucci, “Synthesis, characterization and self cleaning properties of titania nanoparticles grafted on polyester fabrics,” *J. Photochem. Photobiol. A Chem.*, vol. 274, pp. 1–6, 2014.
- [157] B. Tang *et al.*, “Application of anisotropic silver nanoparticles: Multifunctionalization of wool fabric,” *J. Colloid Interface Sci.*, vol. 356, no. 2, pp. 513–518, 2011.

- [158] M. S. Stan *et al.*, “Photocatalytic, Antimicrobial and Biocompatibility Features of Cotton Knit Coated with Fe-N-Doped Titanium Dioxide Nanoparticles,” *Mater. (Basel, Switzerland)*, vol. 9, no. 9, p. 789, Sep. 2016.
- [159] N. Veronovski, A. Rudolf, M. S. Smole, T. Kreže, and J. Geršak, “Self-cleaning and handle properties of TiO₂-modified textiles,” *Fibers Polym.*, vol. 10, no. 4, pp. 551–556, 2009.
- [160] M. S. Azami, W. I. Nawawi, A. H. Jawad, M. A. M. Ishak, and K. Ismail, “N-doped TiO₂ synthesised via microwave induced photocatalytic on RR4 dye removal under LED light irradiation,” *Sains Malaysiana*, vol. 46, no. 8, pp. 1309–1316, 2017.
- [161] N. Nasralla *et al.*, “Structural and spectroscopic study of Fe-doped TiO₂ nanoparticles prepared by sol-gel method,” *Sci. Iran.*, vol. 20, no. 3, pp. 1018–1022, 2013.
- [162] Y. Zhang, Y. Shen, F. Gu, M. Wu, Y. Xie, and J. Zhang, “Applied Surface Science Influence of Fe ions in characteristics and optical properties of mesoporous titanium oxide thin films,” vol. 256, pp. 85–89, 2009.
- [163] S. Sood, A. Umar, S. K. Mehta, and S. K. Kansal, “Highly effective Fe-doped TiO₂ nanoparticles photocatalysts for visible-light driven photocatalytic degradation of toxic organic compounds,” *J. Colloid Interface Sci.*, vol. 450, pp. 213–223, 2015.
- [164] I. Ganesh *et al.*, “Preparation and characterization of Co-doped TiO₂ materials for solar light induced current and photocatalytic applications,” *Mater. Chem. Phys.*, vol. 135, no. 1, pp. 220–234, 2012.
- [165] V. Moradi, M. B. G. Jun, A. Blackburn, and R. A. Herring, “Significant improvement in visible light photocatalytic activity of Fe doped TiO₂ using an acid treatment process,” *Appl. Surf. Sci.*, vol. 427, pp. 791–799, 2018.
- [166] Z. Li, W. Shen, W. He, and X. Zu, “Effect of Fe-doped TiO₂ nanoparticle

derived from modified hydrothermal process on the photocatalytic degradation performance on methylene blue,” vol. 155, pp. 590–594, 2008.

- [167] M. J. Valero-Romero *et al.*, “Photocatalytic properties of TiO₂ and Fe-doped TiO₂ prepared by metal organic framework-mediated synthesis,” *Chem. Eng. J.*, vol. 360, pp. 75–88, 2019.
- [168] B. Xin, Z. Ren, P. Wang, J. Liu, L. Jing, and H. Fu, “Study on the mechanisms of photoinduced carriers separation and recombination for Fe³⁺-TiO₂ photocatalysts,” *Appl. Surf. Sci.*, vol. 253, no. 9, pp. 4390–4395, 2007.
- [169] L. Cai, X. Liao, and B. Shi, “Using collagen fiber as a template to synthesize TiO₂ and Fe_x/TiO₂ Nanofibers and their catalytic behaviors on the visible light-assisted degradation of orange II,” *Ind. Eng. Chem. Res.*, vol. 49, no. 7, pp. 3194–3199, 2010.
- [170] C. Xu *et al.*, “Enhanced mechanism of the photo-thermochemical cycle based on effective Fe-doping TiO₂ films and DFT calculations,” *Appl. Catal. B Environ.*, vol. 204, pp. 324–334, 2017.